Chapitre 1

Joint detection-estimation
in fonctional MRI

1.1. Introduction to functional neuroimaging

The objective of functional neuroimaging is the characterization of the brain in action. Its most conventional use consists of assigning a task to an individual while simultaneously measuring a signal induced by the activity of the brain.

Several investigation modalities allow the neuroscientist to probe the operation of the brain both in healthy volunteers and in patients, whether the pathology is neurodegenerative (Alzheimer), psychiatric (schizophrenia) or neurological (AVC, epilepsy). Without going into the details of a taxonomy of imaging modalities, it is noteworthy to give a general overview (see Fig. 1.1) and distinguish those that allow two fundamental questions to be answered in a simplified form: "where" and "when" do brain processes occur? In fact, the brain is a complex structure where specialization and functional integration coexist, so well it would be an illusion to picture cognitive functions as very localized specialized modules. Among the tools of functional neuroimaging, we quickly discuss the following:

– functional magnetic resonance imaging (fMRI) consists of measuring in a non-invasive manner, BOLD signals[1] which reflects the rate of oxygenation of blood in the brain [OGA 90]. Through a neurovascular response mechanism, the flow of oxygenated blood increases in the regions whose neuronal metabolism increases,

Chapitre rédigé par Philippe Ciuciu, Florence Forbes, Thomas Vincent et Lotfi Chaari.

1. *Blood Oxygenated Level-Dependent.*

in much more significant fashion than necessary. Because of its good spatial resolution (around the mm), by using this method, it is possible to identify the brain regions specifically involved in a given task. Since the 2000s and the emergence of event-related fMRI, which consists in presenting stimuli in an isolated manner in time, it is possible to recover the dynamics of the BOLD signal with a temporal resolution of the order of the second. This is still slower than the dynamics of cognitive processes (a few tens to hundreds of milliseconds). The choice of fMRI as an investigation method is multiple: on the one hand, with the advent of very high-field imagers[2], of parallel imaging [CHA 11b, PRU 99], and compressed sampling techniques [BOY 12, LUS 07], significant gains are still expected in spatio-temporal resolution. On the other hand, the emergence of new contrast agents (CEST, USPIO) could help to achieve a molecular resolution of the order of that attained in PET;
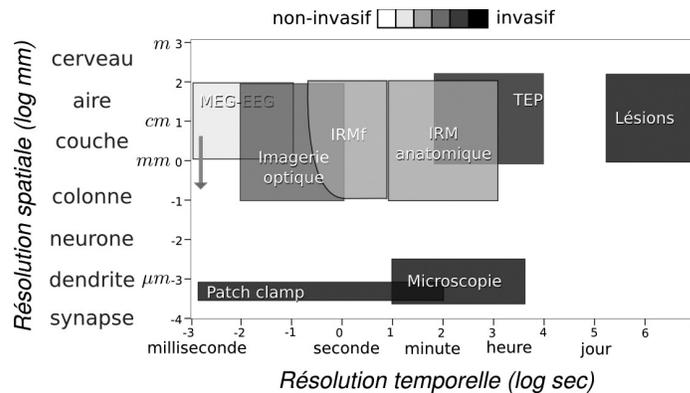
Figure 1.1. *Comparaison of different brain imaging modalities in terms of spatio-temporal resolution and invasiveness degree*

– positron emission tomography (PET) consists of measuring the modifications of blood flow through a radioactive tracer that must first be injected intravenously. The diffusion of the tracer and the modulation of the blood flow being relatively slow phenomena, this technique does not give access to the dynamics of neural mechanisms. Its invasiveness and the low temporal resolution of the observed biological phenomena make it an increasingly less used technique nowadays in functional imaging, supplanted by fMRI;

– electroencephalography (EEG) was the first non-invasive neuroimaging method, developed in 1929, by the neurologist Hans Berger. Unlike previous methods, it is a measure of the electrical activity. EEG is relatively spatially inaccurate but it does offer a good temporal resolution, limited only by the speed of the measurement electronics (5 kHz) [SWA 98]. The conventional approach consists in measuring

---

2. MRI at 11.7 T expected end of 2013 at NeuroSpin.

evoked potentials: repeating the same stimulation a large number of times, it is possible to bring forward positive and negative waves characteristic of the different stages of the information processing procedure (for example, evoked potentials N100, P300, etc.) [HAL 98];

– magnetoencephalography (MEG) provides information relatively similar to the EEG, but it measures magnetic fields induced by the activity of the brain. The significance of MEG lies in the fact that, unlike electric fields, magnetic fields are almost not distorted by their passage through organic tissues (notably the interface between the cerebrospinal fluid and the skull). Just like with EEGs, it is possible with the solution of a linear inverse problem to reconstruct the sources of the electromagnetic signal on the cortical surface. This helps to identify with an accuracy of half a centimeter the regions where evoked fields are issued [SEK 05]. These spatial localization techniques have expanded with the help of regularization tools [BAI 97] and the advent of efficient optimization algorithms [BAU 11, GRA 11].

A key step in the choice of imaging modality lies in the neuroscientific question which must be answered. If the objective is to ensure the temporal decoding of neuronal activity, the best choice seems to be MEG or EEG by default. If on the other hand, spatial localization is being promoted, fMRI seems more sensible. Beyond this choice, obtaining a reliable description of the neuronal activity can be improved, firstly in designing more efficient measurement tools (imagers, sensors), then by improving analysis methods to correct inaccuracies or measurement artifacts (robust reconstruction, denoising, distortions, etc.) or by considering more realistic mathematical models of underlying physiological processes.

This chapter falls precisely under the scope of a restoration and object detection problematics related to brain activity from noisy fMRI signals, by exposing a Bayesian approach to the joint detection-estimation (JDE) of cerebral activity, that is for solving a spatio-temporal inverse problem (3D+time). The JDE approach calls into question the conventional paradigm of activations detections in fMRI by estimating the impulse response of the neurovascular system rather than assuming that it is known and constant through the whole brain.

Afterwards, we present in Section 1.2 the problematics of JDE, then inversion is addressed in a Bayesian framework in Section 1.3. Two alternative inference patterns, that is, stochastic and variational, are then presented in Section 1.4 and 1.5, respectively. A comparison of the results provided by these two approaches, both with simulated and real data, is achieved in Section 1.6, thus initiating a discussion regarding the contributions of each formalism at the end of the chapter.

## 1.2. Joint detection-estimation of brain activity

1.2.1. *Detection and estimation: two interdependent issues*

The objective of the intra-suject fMRI analysis is twofold: on the one hand, (i) to locate the neuronal activity evoked by cognitive tasks of interest during an experimental paradigm, that is to say, to detect voxels activated by stimulation, and on the other hand, (ii) to estimate the dynamics of the neurovascular system which establishes the link between stimulation and measured BOLD signals, by characterizing the haemodynamic response function (HRF) whose canonical form is described in Fig. 1.2. The objective is therefore to create activation maps as well as a local description of the response induced by stimulation, to better understand neurovascular coupling but also to contribute to a dynamic pattern of brain functioning, by considering, for example, the spatial variability of the time taken to reach the peak of the response or by attempting to infer temporal scheduling relationships between activation states.

The usual approach to address these two issues is based on multiple regression, still known as the general linear model (GLM) [FRI 95]. In this context, an experimental design matrix is built, that is to say, a set of regressors representing the activation canonical time courses. These time courses are built as the convolution of canonical HRF (see Fig. 1.2) with the binary signal deducted from each experimental condition present in the paradigm, that is from the signal encoding stimuli occurrences specific to this condition (for example, presentation of a known face): each "1" indicates an instance of the stimulus. The detection is then performed voxel-wise by estimating the GLM parameters with respect to the maximum likelihood and sufficient normalized statistics (e.g. Student test) are then calculated in order to detect activations (difference in activity or contrast between two experimental conditions as the activity in response to familiar *versus* unfamiliar faces) by rejecting the zero hypothesis according to which contrast is zero, with a specified first species risk.

In the framework of the GLM, hemodynamics estimation can only be effected in regions detected as activated. As a result, it become biased because this detection has relied on a predefined canonical model. It appears that these two tasks are highly interdependent: a good HRF model is necessary to build the linear model and to correctly detect activations whereas a reliable estimation of the HRF is only available in correctly detected areas. Although it is possible to inject some temporal flexibility within the linear model [CAS 08, HEN 00] by adding regressors (for example, functions bases) [WOO 04a], derivation and dispersion of the canonical HRF [HEN 00], FIR model [GOU 00], etc.), it is customary in GLM approaches to use only a hemodynamic model fixed for the whole brain, which is contrary to the knowledge about the BOLD signal (see Subsection 1.2.2). Furthermore, estimating the HRF makes sense only in regions activated by a specific task, which induces a preselection bias and does not reflect the hemodynamic activity of the whole brain.

An approach to the voxel-wise HRF estimation [CIU 03, MAR 03] allows sometimes the activation states to be inferred in a second phase. However,. this methodology appears to be sometimes not very robust because of nuisance and noise components prominent in the BOLD signal [CIU 04].
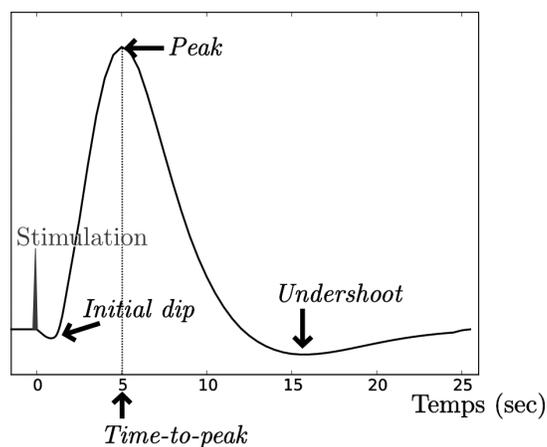
Figure 1.2. *Canonical HRF and its main characteristics. This response performs a delay as well as a slow variation transformation of the input stimulation signal. The* initial dip *or early depletion is not always observed and reflects an immediate extraction of oxygen due to neuronal excitement.*

The idea of performing a joint detection-estimation (JDE) has originally appeared in [MAK 05, MAK 08], where the problem of the reproducibility of the HRF is treated spatially by adopting a 3D brain parcellation (see Fig. 1.3). The objective is thus to bring out a spatial scale where this hemodynamic filter, embodied by the HRF can be locally assumed as constant, so as to make its estimation the most robust possible, unlike voxel-wise attempts [de 08]. It is now necessary to formulate the physiological hypotheses underlying the retained model.
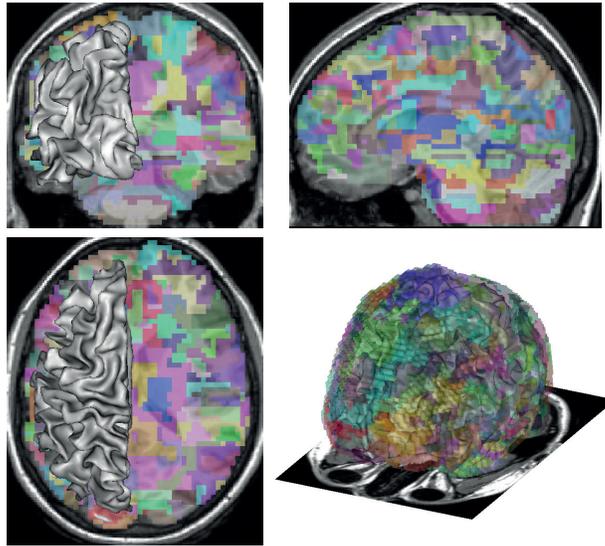
Figure 1.3. *Coronal, sagittal (on top), axial and 3D entire brain (bottom) views*
of an intra-subject parcellation, where a color code for a parcel, superposed
to the anatomical MRI in grayscale as well as to the cortical surface (gray mesh)
(see color annex)

1.2.2. *Hemodynamics physiological hypotheses*

The significant characteristics of the BOLD signal synthesized here consists of all the *a priori* knowledge about the observed signal [LOG 01].

$\mathcal{H}_1$) The signal is very noisy: variations in hemodynamic activity evoked by the paradigm represent only a change in the order of 5 % with respect to the baseline at 3 Tesla.

$\mathcal{H}_2$) There exists a spatial correlation of BOLD signals, due to observed physiological phenomena and network neuronal functioning. These phenomena have a wider spatial support than the spatial resolution of the data.

$\mathcal{H}_3$) The signal presents a short and long-range temporal correlation. The short-range or high-frequency component comes naturally from the duration of physiological phenomena that exceed the sampling period. Among these, some are of interest as related to the paradigm, others reflect physiological regulations that are difficult to explicitly model, due to their unexpected nature. Therefore, they fall under the scope of noise modeling in the form of a temporally autocorrelated random process [WOO 01]. Long-range correlation comes partly from artifacts: respiratory and above

all cardiac pulsations have higher frequencies than those of the measurement of the signal. The Shannon-Nyquist condition is not satisfied, thus inducing spectral aliasing of cardiac and respiratory components in the low frequencies of the acquired signals. In its very low frequency part, the long range component is also associated with intrinsic cerebral activity of interest that can be highlighted in MRIf in rest functional networks (for example, default mode) [CIU 08, LIN 01, ZAR 97].

$\mathcal{H}_4$) If neurovascular coupling can be physiologically described by the neurovascular complex, the origin of the measured BOLD signal remains unclear and depends on variations of several factors: blood volume, blood flow and deoxyhemoglobin concentration, without being able to clearly establish the contributions of each one of them [EKS 10, LOG 01].

$\mathcal{H}_5$) Hemodynamics spatially varies, both within a same subject [HAN 04, MIE 00] and between subjects [AGU 98, BUC 98]. Inter-subject variations are even more pronounced when populations that can differ in age [RIC 03], in pathology or in therapeutics [D'E 99] are considered.

The balloon model [BUX 98] and its extensions [BUX 04, RIE 04] are those that from a physiological point of view establish the finest description of neurovascular coupling following hypotheses $\mathcal{H}_1$-$\mathcal{H}_5$. Governed by systems of non-linear differential equations with unknown parameters, these models suffer from identifiability problems and proved to be difficult to put into practice in fast multicondition event-based paradigms. We rather consider in this chapter a convolutive model, more easily manipulable but also able to cover a wider range of paradigms. Below, we recall temporal hypotheses characteristic of the BOLD signal which allow the implementation of this model.

1.2.3. *Space variable convolutive model*

Stationnarity. The BOLD response is assumed to be stationary in time, that is not varying in different tests of a same stimulus: if given $x(t)$ a stimulus presented at time t and $h(x(t))$ the evoked hemodynamic response, then stationarity indicates: $h(x(t+\Delta t)) = h(x(t))$ for Δt an interstimulus interval such as $\Delta t > 3$ s. Conversely, response saturation phenomena are involved and the response becomes sub-linear [BUC 98, DAL 97].

From a physiological point of view, this hypothesis is justified by the construction of the paradigm where care is taken to pseudo-randomly distribute tests to prevent learning or anticipating and limit the duration of the experiment to avoid fatigue in the subject. A second justification comes from the raised cognitive question: a response reproducible through testing is looked for.

Linearity. The vascular system is assumed to be linear which amounts to assume on the one hand, that $h(ax(t)) = ah(x(t))$ for an amplitude $a > 0$ of the stimulus, and

$n \in \mathbb{N}_N^* = \{1, \ldots, N\}$	Scans index
$j \in \mathbb{N}_J^*$	Voxels index
RT	Repetition time: data temporal resolution
$\mathbb{V} = \{V_j\}_{j=1:J}$	Voxels set. For whole brain analysis, $J \approx 5.10^4$. For regional analysis, $J \approx 500$.
$m \in \mathbb{N}_M^*$	Experimental conditions index
$\boldsymbol{y}_j = (y_{j,n})_{n=1:N} \in \mathbb{R}^N$	fMRI signal measured at voxel V_j
$\boldsymbol{b}_j = (b_{j,n})_{n=1:N} \in \mathbb{R}^N$	Noise measurement at voxel V_j
$\boldsymbol{Y} = (\boldsymbol{y}_j)_{j=1:J}$	$N \times J$ acquired data matrix for $\mathbb{V}$
$\boldsymbol{\ell}_j = (\ell_{j,n})_{n=1:N} \in \mathbb{R}^Q$	Low frequency derivative coefficients at V_j
$\boldsymbol{L} = (\boldsymbol{\ell}_j)_{j=1:J}$	$Q \times N$ derivative coefficients matrix for $\mathbb{V}$
$\boldsymbol{q}^m = (q_j^m)_{j=1:J}$	Activation states for $\mathbb{V}$ associated to the condition m
$\boldsymbol{Q} = (\boldsymbol{q}^m)^{m=1:M}$	State matrix for all conditions and $\mathbb{V}$
$\boldsymbol{a}^m = (a_j^m)_{j=1:J}$	NRL for $\mathbb{V}$ associated to the condition m
$\boldsymbol{A} = (\boldsymbol{a}^m)^{m=1:M}$	NRL matrix for all conditions and $\mathbb{V}$
$\boldsymbol{x}_m = (x_m^{dt})^{dt=0:\Delta t:\frac{N \times TR}{\Delta t}}$	Sequence encoding the arrival times of stimuli m sampled on a resolution grid Δt
$\boldsymbol{h}_\gamma = (h_\gamma^{d\Delta t})^{d=0:D}$	HRF with Δt the sampling period of HRF

Tableau 1.1. *Notation table*

on the other hand, that it is additive with respect to experimental conditions, noted here x_1 and x_2: $h(x_1(t) + x_2(t)) = h(x_1(t)) + h(x_2(t))$. However, a number of saturation phenomena exist. Thus, for a doubling of the intensity of sound stimulus, the response in the auditory cortex does only double in a restricted volume range in decibels.

These hypotheses lead to a convolutional system, which is in addition justified by the choice of a simple model but respecting the hypotheses $\mathcal{H}_1$-$\mathcal{H}_4$. In order to ensure a certain flexibility, a linear finite impulse response (FIR) filter is retained so as to formulate its identification as a non-parametric estimation problem. On the other hand, in order to account for $\mathcal{H}_5$ while ensuring a parsimonious character and therefore a larger robustness of estimation, we have proposed the following restrictions [MAK 05, MAK 08]: "a single HRF form by region characterizes the hemodynamic system, local variations of activity at the voxel level are reduced to amplitude modulations of the HRF only. The model therefore decouples the form of the hemodynamic filter of its amplitude, inducing a bilinear system".

We are now introducing the notations used subsequently in the text. Table 1.1 indicates the variables associated with quantities of interest using the following conventions: vectors[3] and matrices are noted in lowercase and uppercase bold,

respectively (example $\boldsymbol{x}$ et $\boldsymbol{X}$). Scalars are noted in lowercase regular characters characters and sets with double-bars (example $\mathbb{V}$), transposition is symbolized by $^{\text{t}}$.

1.2.4. *Regional generative model*

The approach assumes a prior partitioning of data, that is to say, parcellation guaranteeing hemodynamic homogeneity within each parcel. Thus assuming the brain previously subdivided into $\boldsymbol{\mathcal{P}} = (\mathcal{P}_\gamma)_{\gamma=1:\Gamma}$ parcels, each having homogeneous functional properties from the perspective of hemodynamics. The proposed model will therefore be inferred parcel-wise, each one independently from the others.

Each parcel $\mathcal{P}_\gamma$ is defined by a connected set of voxels $\mathbb{V}_\gamma$. It has a unique HRF $\boldsymbol{h}_\gamma$ characteristic of $\mathcal{P}_\gamma$, which is thus considered identical for all voxels. Activation levels $\boldsymbol{A}$ are unique to each voxel V_j and each experimental condition m (see BOLD reponse stationarity hypothesis). In can be derived that in each voxel $V_j \in \mathbb{V}_\gamma$ the following generative model, shown in figure 1.4:

$$\boldsymbol{y}_j = \boldsymbol{S}_j \boldsymbol{h}_\gamma + \boldsymbol{P}\boldsymbol{\ell}_j + \boldsymbol{b}_j, \quad \text{with} \quad \boldsymbol{S}_j = \sum_{m=1}^{M} a_j^m \boldsymbol{X}_m \qquad [1.1]$$

where $\boldsymbol{S}_j \boldsymbol{h}_\gamma$ is the sum of the stimulus components induced from the BOLD signal. Matrix $\boldsymbol{X}_m = (x_m^{n-d\Delta t})_{n=1:N}^{d=0:D}$ is binary, of dimensions $N \times (D+1)$, and code occurrences of stimuli of the m-th condition. The parameter Δt is the unknown HRF sampling period $\boldsymbol{h}_\gamma$ in $\mathcal{P}_\gamma$. The scalar a_j^m is the amplitude of the response at voxel V_j for the condition m. These weights model the transition between stimulation and vascular response. They can therefore be considered as "pre-vascular". In addition, since it is admitted that the occurrence of a stimulus coincides with neuronal excitation, itself at the origin of the vascular response, amplitudes $\boldsymbol{A}$ are therefore referred to as "neural response levels"(NRL). Matrix $\boldsymbol{P}$ is an orthogonal basis of low frequency functions of size $N \times Q$. At each voxel, a weight vector $\boldsymbol{\ell}_j$ is attached in order to estimate the derivative. The set of these vectors within $\mathcal{P}_\gamma$ is grouped in $\boldsymbol{L}$. Finally, $\boldsymbol{b}_j$ is the noise vector in V_j whose structure is detailed in Subsection 1.3.1.

---

3. Always in column.
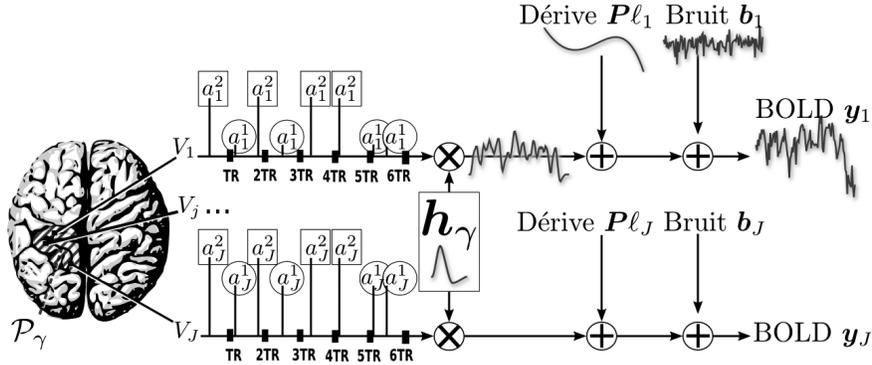
Figure 1.4. *Parcel-wise model of the BOLD signal. The size of each parcel $\mathcal{P}_\gamma$ is typically of some hundreds of voxels. The number M of experimental conditions of a paradigm usually varies between 1 and 5; in this illustration, $M = 2$. This model supports asynchronous paradigms for which the arrival times of the stimuli do not necessarily correspond to the acquisition times. The NRL (a_j^1, a_j^2) are voxel-specific whereas the HRF h_γ is constant for the parcel $\mathcal{P}_\gamma$ but varies from one parcel to another (not shown). It can be sampled at a period of $0.5\,s$ for a period ranging typically from $20\,s$ to $25\,s$ (for example $D = 51$). The coefficients ℓ_j usually focus on a few composantes ($Q = 4$).*

1.3. Bayesian approach

Bayesian formalism requires melting the problem in a probabilistic framework and the main object of interest is the joint *a posteriori* density of all the unknown parameters knowing observations $\boldsymbol{Y}$. This latter allows the proposal of estimators of the unknowns, particularly for $(\boldsymbol{h}_\gamma, \boldsymbol{A})$ that are the most relevant from a cognitive perspective. It is defined by:

$$p(\boldsymbol{h}_\gamma, \boldsymbol{A}, \boldsymbol{L}, \boldsymbol{\Theta} \mid \boldsymbol{Y}) \propto p(\boldsymbol{Y} \mid \boldsymbol{h}_\gamma, \boldsymbol{A}, \boldsymbol{L}, \boldsymbol{\theta}_0)\, p(\boldsymbol{A} \mid \boldsymbol{\theta_A})\, p(\boldsymbol{h}_\gamma \mid \boldsymbol{\theta_h}) p(\boldsymbol{L} \mid \boldsymbol{\theta_\ell})\, p(\boldsymbol{\Theta})$$

$$[1.2]$$

where $\boldsymbol{\Theta}$ gathers all the hyperparameters of the model: $\boldsymbol{\theta}_0$ contains those related to the noise model and $\boldsymbol{\theta_x}$ concerns those related to the unknown $\boldsymbol{x} \in \{\boldsymbol{h}_\gamma, \boldsymbol{A}, \boldsymbol{L}\}$. This joint density requires the expression of the likelihood term as well as the *a priori* definition of the modelised variables.

1.3.1. *Likelihood*

Likelihood is the density of the observations for a set of given parameters of the concerned model. It models the uncertainty of the model to fit the observed data and therefore is directly dependent on the hypotheses of the noise. Even if the structure

of the noise is spatially correlated [WOO 04b], this dependency is negligible and fMRI time-series are considered spatially independent but non-identically distributed. Moreover, given the nature of the acquisition of data (see $\mathcal{H}_2$), noise is supposed to be temporally autocorrelated and in this case, an AR(1) process is considered following [WOO 01]: $\boldsymbol{b}_j \sim \mathcal{N}(\boldsymbol{0},\boldsymbol{\Gamma}_j)$ with $\boldsymbol{\Gamma}_j = \sigma_j^2 \boldsymbol{\Lambda}_j^{-1}$ and where $\boldsymbol{\Lambda}_j$ is tridiagonal symmetric and depends on the AR parameter ρ_j [MAK 08]: $(\boldsymbol{\Lambda}_j)_{1,1} = (\boldsymbol{\Lambda}_j)_{N,N} = 1$, $(\boldsymbol{\Lambda}_j)_{p,p} = 1 + \rho_j^2$ for $p = 2 : N - 1$ and $(\boldsymbol{\Lambda}_j)_{p+1,p} = (\boldsymbol{\Lambda}_j)_{p,p+1} = -\rho_j$ for $p = 1 : N - 1$. These parameters are supposed to be variable from a voxel V_j to another given their dependence to tissue [WOO 04a, PEN 07]. The likelihood is then written:

$$p(\boldsymbol{Y} \,|\, \boldsymbol{h}_\gamma, \boldsymbol{A}, \boldsymbol{L}, \boldsymbol{\theta}_0) \propto \prod_{j=1}^{J_\gamma} |\boldsymbol{\Gamma}_j|^{-1/2} \exp\left(-\frac{1}{2} \overline{\boldsymbol{y}}_j^{\mathrm{t}} \boldsymbol{\Gamma}_j^{-1} \overline{\boldsymbol{y}}_j\right) \qquad [1.3]$$

where $\boldsymbol{\theta}_0 = (\theta_{0,j})_{j=1:J_\gamma}$, $\theta_{0,j} = (\rho_j, \sigma_j^2)$ and $\overline{\boldsymbol{y}}_j = \boldsymbol{y}_j - \boldsymbol{P}\boldsymbol{\ell}_j - \boldsymbol{S}_j \boldsymbol{h}_\gamma$.

1.3.2. A priori *distributions*

In the Bayesian approach, *a priori* distributions are introduced for the unknown $(\boldsymbol{A}, \boldsymbol{h}_\gamma, \boldsymbol{L})$ and for the hyperparameters $\boldsymbol{\Theta}$.

1.3.2.1. *Hemodynamic response function (HRF)*

Following [CIU 03, MAR 03], an HRF with smooth variations is expected, its *a priori* density is a multivariate Gaussian distribution whose variance-covariance matrix expresses a constraint of the second derivative: $\boldsymbol{h}_\gamma \sim \mathcal{N}(\boldsymbol{0}, v_h \boldsymbol{R})$ with $\boldsymbol{R} = (\boldsymbol{D}_2^{\mathrm{t}} \boldsymbol{D}_2)^{-1}$. The aim is to penalize large slope variations. Boundary constraints are also introduced in the form $h_0 = h_{D\Delta t} = 0$. The *a priori* retained for variance $v_{\boldsymbol{h}}$ corresponds to the Jeffreys *a priori*: $p(v_{\boldsymbol{h}}) = v_{\boldsymbol{h}}^{-1/2}$. On the sole basis of this *a priori*, in an inactive parcel, it can be derived that the estimated hemodynamic response will be of very low amplitude, and therefore also its slope. It will thus have a strong likelihood. Several solutions are conceivable to avoid in the case of inactive signals that a HRF solution is aberrant, hence making believe that it is an active signal. One of them consists of replacing the mean Gaussian vector by imposing it to a form similar to canonical hemodynamics. Another consists in detecting the active parcels after inference, that is to say, for which at least one experimental condition is relevant that is that it delivers significant evoked response or positive NRLs [BAK 12].

1.3.2.2. *Neural response levels (NRL)*

In accordance with the principle of maximum entropy [ROB 07, p. 109], the independance of the NRLs is postulated between conditions: $p(\boldsymbol{A} \,|\, \boldsymbol{\theta}_{\boldsymbol{a}}) = \prod_m p(\boldsymbol{a}^m \,|\, \boldsymbol{\theta}_m)$ with $\boldsymbol{\theta}_{\boldsymbol{a}} = (\boldsymbol{\theta}_m)_{m=1:M}$ grouping the set of hyperparameters for the m-th condition. Mixing models are introduced to segment activated voxels from non-activated voxels.

Given q_j^m the allocation variables that encode the activated ($q_j^m = 1$) or non-activated ($q_j^m = 0$) state for the condition m within voxel V_j. NRLs remain independent conditionally on $\boldsymbol{q}^m$: $p(\boldsymbol{a}^m \mid \boldsymbol{q}^m, \boldsymbol{\theta}_m) = \prod_j p(a_j^m \mid q_j^m, \boldsymbol{\theta}_m)$.

Spatial mixture models (SMM) introduced in [VIN 10a] allow accounting for a certain spatial correlation between neighboring voxels in order to facilitate the detection of clusters of activation rather than isolated voxels. In SMMs, the mixture weights are implicit and controlled only by the local interaction relationship between latent variables. The marginal distribution of the NRLs, not factorizable with voxels, is written as follows:

$$p(\boldsymbol{a}^m \mid \boldsymbol{\theta}_m) = \sum_{\boldsymbol{q}^m \in \{0,1\}^{J_\gamma}} \Pr(\boldsymbol{q}^m \mid \boldsymbol{\theta}_m) \prod_{j=1}^{J_\gamma} p(a_j^m \mid q_j^m, \boldsymbol{\theta}_m) \qquad [1.4]$$

Fortunately, as we shall see in Section 1.4, its explicit expression is not necessary since only conditional laws are useful in the sampling scheme.

Spatial correlation is directly taken into account in the activation probability by means of a hidden Ising field[4] of the variables $\boldsymbol{q}^m$, according to previous works [HIG 98, SMI 03]. Here, the *a priori* field of $\boldsymbol{q}^m$ is expressed in the form:

$$\Pr(\boldsymbol{q}^m \mid \beta_m) = Z(\beta_m)^{-1} \exp\big(\beta_m U(\boldsymbol{q}^m)\big) \quad \text{where} \quad U(\boldsymbol{q}^m) = \sum_{j \sim k} I(q_j^m = q_k^m)$$

$$[1.5]$$

and $I(A) = 1$ if A true and $I(A) = 0$ otherwise. The notation $j \sim k$ means that the sum extends over all pairs (V_j, V_k) of neighbouring voxels. The neighbourhood system can be 3D in the cerebral volume intersecting parcel $\mathcal{P}_\gamma$ or 2D along the cortical surface. In this chapter, we only discuss the 3D case using 6-connectedness. The extensions to 18 and 26 neighbours are direct. In [1.5], we do not consider external fields in order to not promote an *a priori* state. Nevertheless, previous works have showed that anatomical information could be modeled through an external field such that to increase the likelihood of activation (classe 1) in gray matter [SMI 03]. The parameter $\beta_m > 0$ controls the level of spatial regularization: a large value of β_m associates high probabilities to homogeneous configurations, that is to say, containing voxels of the same class. It should be noted that activation patterns within a parcel $\mathcal{P}_\gamma$ are likely to vary from a condition m to the other. That is why different parameters β_m are considered. The partition function (FP) $Z(\cdot)$ of the Markov field is written:

$$Z(\beta_m) = \sum_{\boldsymbol{q}^m \in \{0,1\}^{J_\gamma}} \exp\big(\beta_m U(\boldsymbol{q}^m)\big) \qquad [1.6]$$

---

4. It should be noted that if the aim is to manage deactivations, 3-class Potts fields are substituted to the Ising fields (see [RIS 11] for details).

and ensures the normalization of the probability $\Pr(\boldsymbol{q}^m \mid \beta_m)$. In the following, we assume that $(a_j^m \mid q_j^m = i) \sim \mathcal{N}(\mu_{i,m}, v_{i,m})$, for $i = 0,1$. We impose $\mu_{0,m} = 0$ for the average of NRLs in inactive voxels leading to the hyperparameters vector $\boldsymbol{\theta}_m = [v_{0,m}, \mu_{1,m}, v_{1,m}, \beta_m]$ for each condition m.

We should observe that a similar formulation such as Bernoulli-Gaussian has also been proposed in fMRI in [SMI 03]. This situation corresponds to the case of degenerate mixing, that is to say, $v_{0,m} = 0$. However, this formulation is too coarse, as different configurations of activation can appear in the current parcel and the mixing parameters $\boldsymbol{\theta}_m$ for the condition m are supposed to adapt themselves to this latter set:

– in the case where all voxels are activated as a result of the condition m, the proposed model is too rich and therefore the estimation of $v_{0,m}$ tends towards 0. Once again, the BG model reappears without having imposed it;

– in the case where all voxels are inactivated, the estimate of $\mu_{1,m}$ is close to 0 and the two mixing classes are superimposed. There again, the model is too rich, and the approach developed in [BAK 12] for the automatic selection of relevant conditions provides an effective solution to this problem. Considering a BG model would not add anything in this case, because it would also be redundant;

– in the intermediate case where only a part of the voxels is activated in response to the condition m, the proposed mixing model can adapt itself to heterogeneous configurations and leads to consider as inactive weakly activated voxels with regard to the others present in the parcel. It is in this kind of configurations that the BG model is questioned because it can lead to false positives. The introduction of a variance $v_{0,m} \neq 0$ therefore helps to not bring the estimation $\mu_{1,m}$ close to 0 by excluding activated voxels (those whose evoked activity is too low);

– in the presence of light deactivations[5], that is negative NRLs, the BG model is also considered in default and there again, the proposed formulation, more flexible, adapts itself to this configuration provided that the number of deactivations and their amplitude is low faced with those of activations, in order to keep $\mu_{1,m} > 0$;

– richer three-class mixing models and considering support distributions in $\mathbb{R}_+$ or $\mathbb{R}_-$ for NRLs of activated and deactivated voxels have been successfully tested in [MAK 08] but the generated numerical complexity does not easily consider the introduction of spatial models with an autodidact estimation of the parameters.

It is interesting to observe that the spatial regularization introduced in $\boldsymbol{A}$ is non-quadratic due to the introduction of a composite model of $(\boldsymbol{A}, \boldsymbol{Q})$, it therefore enables raising the activation boundaries on the furrow walls within the cortex, in a simpler manner than through the use of convex non-quadratic regularization directly

---

5. Well known phenomena brought forward in the functional network of the mode by default [CIU 12, FOX 07, GRE 03], where the level of activity decreases as a result of the action of a stimulus.

applied to $\boldsymbol{A}$. The reason is due to the fact that the automatic estimation of the regularization level β_m does only involve the *a priori* Ising or Potts field whose partition function calculation can be tabulated in advance because the variables $\boldsymbol{Q}$ are hidden: they are therefore not intervening in the observation model [1.1]. Moreover, the regulation remains separable through the experimental conditions, whereas a direct regularization on each vector $\boldsymbol{a}^m$ would induce non-separability due to the shape of the observation model.

1.3.2.3. *Mixing hyperparameters*

We consider *a priori* conjugate distributions for variances $v_{0,m}$ and $v_{1,m}$, that is to say, inverse-gamma distributions, $\mathcal{IG}(a_{v_0}, b_{v_0})$ and $\mathcal{IG}(a_{v_1}, b_{v_1})$, identical for all conditions m. The adjustment of the meta-hyperparameters $(a_{v_{0,1}}, b_{v_{0,1}})$ must be carried out by taking care to be the least informative as possible. Besides the fact that the *a posteriori* conditional distribution remains conjugate inverse-gamma, the significance of this choice lies in the fact that it remains clean. Thus, sampling conditional *a posteriori* distributions of variances $v_{\cdot,m}$ is still possible even when one of the mixing classes is empty or consists of a single element, in contrast to the situation generated by the use of non-informative Jeffreys *a priori*, that is of a distribution $p(v_{0,m}) = v_{0,m}^{-1/2}$. For the same reasons, a clean *a priori* $\mathcal{N}(a_{\mu_1}, b_{\mu_1})$ is retained for $\mu_{1,m}$. The choices of constants (a_{μ_1}, b_{μ_1}) are effected to express diffuse densities, that is slightly informative.

1.3.2.4. *Noise and derivatives*

The parameters of noise and derivative, $\boldsymbol{\theta}_0$ and $\boldsymbol{L}$ respectively, are supposed to be spatially independent: $p(\boldsymbol{\theta}_0, \boldsymbol{L} \,|\, v_{\boldsymbol{\ell}}) = \prod_j p(\theta_{0,j}) \, p(\boldsymbol{\ell}_j \,|\, v_{\boldsymbol{\ell}})$ and without *a priori* information, the following is chosen: $\boldsymbol{\ell}_j \sim \mathcal{N}(\boldsymbol{0}, v_{\boldsymbol{\ell}} \boldsymbol{I}_Q)$[6] and $p(\rho_j, \sigma_j^2) = \sigma_j^{-1} I(|\rho_j| < 1)$ in order to ensure the stability of the AR(1) process for the noise [KAY 88]. As with $v_{\boldsymbol{h}}$, we choose a non-informative Jeffreys *a priori* for $v_{\boldsymbol{\ell}}$: $p(v_{\boldsymbol{\ell}}) = v_{\boldsymbol{\ell}}^{-1/2}$.

1.3.3. **A posteriori** *distribution*

From the equations [1.2]–[1.3], and defined *a priori* distributions, we get the *a posteriori* distribution:

$$p(\boldsymbol{h}_\gamma, \boldsymbol{A}, \boldsymbol{L}, \boldsymbol{Q}, \boldsymbol{\Theta} \,|\, \boldsymbol{Y}) \propto p(\boldsymbol{Y} \,|\, \boldsymbol{h}_\gamma, \boldsymbol{A}, \boldsymbol{L}, \boldsymbol{\theta}_0) \, p(\boldsymbol{A}, \boldsymbol{Q} \,|\, \boldsymbol{\theta}_{\boldsymbol{A}}) \, p(\boldsymbol{h}_\gamma \,|\, v_{\boldsymbol{h}})$$
$$p(\boldsymbol{L} \,|\, v_{\boldsymbol{\ell}}) \, p(\boldsymbol{\theta}_0) \, p(\boldsymbol{\theta}_{\boldsymbol{A}}) \, p(v_{\boldsymbol{h}}) \, p(v_{\boldsymbol{\ell}})$$

---

6. Where $\boldsymbol{I}_Q$ is the size Q identity matrix.

that is developed as follows:

$$p(\boldsymbol{h}_\gamma, \boldsymbol{A}, \boldsymbol{L}, \boldsymbol{Q}, \boldsymbol{\Theta} \,|\, \boldsymbol{Y}) \propto v_{\boldsymbol{h}}^{-D/2} v_{\boldsymbol{\ell}}^{-J_\gamma Q/2} \prod_{j=1}^{J_\gamma} (1-\rho_j^2)^{1/2} \sigma_j^{-N-1} I(|\rho_j| < 1)$$

$$\exp\left(-\frac{\boldsymbol{h}_\gamma^{\mathrm{t}} \boldsymbol{R}^{-1} \boldsymbol{h}_\gamma}{2v_{\boldsymbol{h}}} - \sum_{j=1}^{J_\gamma} \left(\frac{\overline{\boldsymbol{y}}_j^{\mathrm{t}} \boldsymbol{\Lambda}_j \overline{\boldsymbol{y}}_j}{2\sigma_j^2} + \frac{\|\boldsymbol{\ell}_j\|^2}{2v_{\boldsymbol{\ell}}}\right)\right) \qquad [1.7]$$

$$\prod_{m=1}^{M} p(\boldsymbol{a}^m \,|\, \boldsymbol{q}^m, \boldsymbol{\theta}_m) p(\boldsymbol{q}^m, \boldsymbol{\theta}_m)$$

It appears in [1.7] that this *a posteriori* distribution is specific to $\mathcal{P}_\gamma$ through the HRF $\boldsymbol{h}_\gamma$. This density is however too complex to allow the analytical calculation of an estimator. Consequently, we exploit in Section 1.4 stochastic simulation tools, still called Markov Chain Monte-Carlo (MCMC) methods to simulate samples from [1.7]. A variational alternative is then presented in Section 1.5.

1.4. Schema for stochastic MCMCinference

The inference scheme revolves around a hybrid Gibbs-Metropolis sampler in which conditional *a posteriori* distributions are sampled in turn, either directly (Gibbs) or using an instrumental distribution (Metropolis-Hastings). The algorithm is detailed in [VIN 10a, table I]. After convergence of the Markov chain, the quantities of interest are then estimated with regard to the *a posteriori* (PM for *Posterior Mean*) as follows: $\forall x \in \{\boldsymbol{h}_\gamma, \boldsymbol{A}, \boldsymbol{\Theta}\}$: $\widehat{x}^{\mathrm{MP}} = (T_{\mathrm{c}} - T_0)^{-1} \sum_{t=T_0+1}^{T_c} x^{(t)}$, where T_0 defines the warming period and T_c the convergence number of iterations. For detection, we use the estimator of the maximum marginal *a posteriori*: $(\widehat{q}_j^m)^{\mathrm{MMAP}} = \arg\max_i \Pr(q_j^m = i \,|\, \boldsymbol{y}_j)$.

Briefly, we present the two stages of the simulation of $\boldsymbol{h}_\gamma$ and of $\boldsymbol{A}$, in order to highlight the links between the variational and stochastisc schemes.

1.4.1. *HRF and NRLs simulation*

The *a posteriori* distribution $p(\boldsymbol{h}_\gamma \,|\, \boldsymbol{Y}, \boldsymbol{A}, \boldsymbol{L}, \boldsymbol{\Theta})$ is Gaussian and is written $\mathcal{N}(\boldsymbol{\mu}_{\boldsymbol{h}_\gamma}, \boldsymbol{\Sigma}_{\boldsymbol{h}_\gamma})$[7]:

$$\boldsymbol{\Sigma}_{\boldsymbol{h}_\gamma}^{-1} = v_{\boldsymbol{h}}^{-1} \boldsymbol{R}^{-1} + \sum_{j=1}^{J_\gamma} \boldsymbol{S}_j^{\mathrm{t}} \boldsymbol{\Gamma}_j^{-1} \boldsymbol{S}_j, \quad \boldsymbol{\mu}_{\boldsymbol{h}_\gamma} = \boldsymbol{\Sigma}_{\boldsymbol{h}_\gamma} \sum_{j=1}^{J_\gamma} \boldsymbol{S}_j^{\mathrm{t}} \boldsymbol{\Gamma}_j^{-1} \big(\boldsymbol{y}_j - \boldsymbol{P}\boldsymbol{\ell}_j\big) \qquad [1.8]$$

---

7. The authors report an error in the expression of $\boldsymbol{\Sigma}_{\boldsymbol{h}}^{-1}$ in [MAK 08, equation (B.1)].

Similarly, by an argument of conjugation, the *a priori* distribution [1.4] of the NRLs $\boldsymbol{A}$ being Gaussian mixture and the likelihood of $\boldsymbol{A}$ being Gaussian when $\boldsymbol{h}_\gamma$ is fixed, the *a posteriori* marginal density $p(\boldsymbol{A}\,|\,\boldsymbol{Y},\boldsymbol{h}_\gamma,\boldsymbol{L},\boldsymbol{\Theta})$ is also Gaussian mixture. Given the introduction of $\boldsymbol{Q}$ in the sampling schema[8] and the spatial correlation model retained in [1.5], the simulation of $\boldsymbol{A}$ is simplified and factorized: $p(\boldsymbol{A}\,|\,\boldsymbol{Y},\boldsymbol{Q},\boldsymbol{h}_\gamma,\boldsymbol{\Theta}) \;=\; \prod_j p(\boldsymbol{a}_j\,|\,\boldsymbol{y}_j,\boldsymbol{q}_j,\boldsymbol{h}_\gamma,\boldsymbol{\Theta})$. Within the voxel V_j, the last thing is to successively consider the different experimental conditions $m \in \mathbb{N}_M^*$ and to simulate according to $p(a_j^m\,|\,q_j^m = i,\boldsymbol{y}_j,\cdots) = \mathcal{N}\!\left(\mu_{i,j}^m,v_{i,j}^m\right)$. The identification of the parameters $(\mu_{i,j}^m,v_{i,j}^m)$ of the Gaussian distributions leads to:

$$v_{i,j}^m = \left(v_{i,m}^{-1} + \boldsymbol{g}_m^{\mathrm{t}}\boldsymbol{\Gamma}_j^{-1}\boldsymbol{g}_m\right)^{-1}, \quad \mu_{i,j}^m = v_{i,j}^m\left(\boldsymbol{g}_m^{\mathrm{t}}\boldsymbol{\Gamma}_j^{-1}\boldsymbol{e}_{m,j} + i\,\mu_{i,m}v_{i,m}^{-1}\right) \qquad [1.9]$$

where $\boldsymbol{g}_m = \boldsymbol{X}_m\boldsymbol{h}_\gamma$ and $\boldsymbol{e}_{m,j} = \boldsymbol{y}_j - \boldsymbol{P}\boldsymbol{\ell}_j - \sum_{m'\neq m} a_j^{m'}\boldsymbol{g}_{m'} = \overline{\boldsymbol{y}}_j + \boldsymbol{g}_m$. The identification of the weights $\lambda_{i,j}^m$ of the *a posteriori* mixture is detailed in [VIN 10a, annexe B].

1.4.2. *Unsupervised spatial and spatially adaptive regularization*

Within a parcel $\mathcal{P}_\gamma$, unsupervised spatial regularization consists of automatically adjusting the vector $\boldsymbol{\beta}$ from data $\boldsymbol{Y}$. With the proposed Gibbs sampler, this step is performed by probabilizing $\boldsymbol{\beta}$ and by adding a sampling step of $p(\boldsymbol{\beta}\,|\,\boldsymbol{Q})$, which depends on $p(\boldsymbol{q}^m\,|\,\beta_m)$ and on the *a priori* $p(\boldsymbol{\beta})$:

$$p(\boldsymbol{\beta}\,|\,\boldsymbol{Q}) = \prod_{m=1}^{M} p(\beta_m\,|\,\boldsymbol{q}^m) \propto \prod_{m=1}^{M} Z(\beta_m)^{-1}\exp\!\left(\beta_m U(\boldsymbol{q}^m)\right)p(\beta_m) \quad [1.10]$$

where $p(\beta_m)$ is chosen truncated on an interval $[0,\beta_{\max}]$ such that to avoid phase transition phenomena. The distribution [1.10] depends on $Z(\cdot)$, independent of m. As a result, the estimation of $Z(\cdot)$ remains a prerequisite to any sampling attempt of $p(\beta_m\,|\,\boldsymbol{q}^m)$. In [VIN 10a], a Metropolis-Hastings algorithm was implemented to perform this step. The acceptance likelihood of a candidate value $\beta_m^{(c)}$ is written: $\alpha(\beta_m^{(t)} \to \beta_m^{(c)}) = \min(1, A_{t\to c}^m)$ where the acceptance ratio $A_{t\to c}^m$ is given by:

$$A_{t\to c}^m = \frac{p(\beta_m^{(c)}|\boldsymbol{q}_m^{(t)})g(\beta_m^{(t)}|\beta_m^{(c)})}{p(\beta_m^{(t)}|\boldsymbol{q}_m^{(t)})g(\beta_m^{(c)}|\beta_m^{(t)})} = \frac{Z(\beta_m^{(t)})}{Z(\beta_m^{(c)})}\exp\left((\beta_m^{(c)} - \beta_m^{(t)})U((\boldsymbol{q}^m)^{(t)})\right)B_{t\to c}^m$$

with $B_{t\to c}^m$ function the instrumental distribution g. The exact evaluation of $Z(\beta)$ in a reasonable time is impossible for conventional images sizes. Its accurate estimation is accessible by adopting a significant sampling scheme on a discrete grid of values of β. However, the computational cost remains important during a whole brain scan

---

8. See details in [VIN 10a, annexe B].

involving multiple parcels for each of which the FP of the hidden field must be estimated. As a matter of fact, these plots have all different sizes and geometries as it is illustrated in Fig. 1.5.

To overcome this difficulty, an FP extrapolation scheme is implemented, relying on a few reference functions to adapt itself to geometry variations. The algorithmic details are available in [RIS 11, VIN 10a].
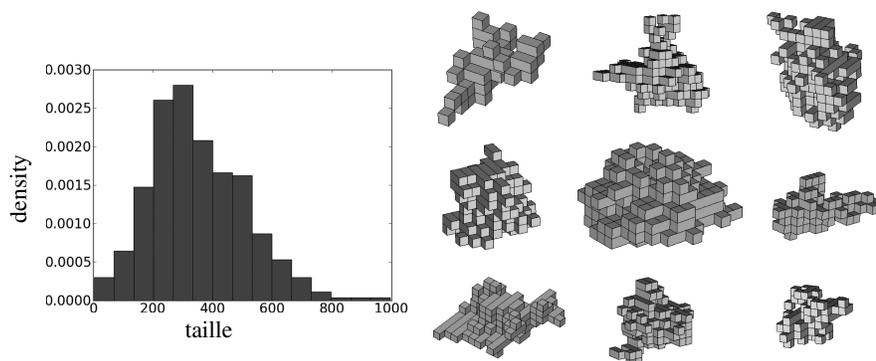
Figure 1.5. *Variability of parcels resulting from real data, forming the input parcellation of the JDE approach. Left: histogram of parcels sizes; right: illustration of a few parcels with varied geometries*

1.5. Alternative variational inference schema

1.5.1. *Motivations and foundations*

The exact Bayesian analysis of the JDE model is difficult and has lead to the approximated calculation of the *a posteriori* distribution [1.7] with the help of an MCMC process, whose asymptotic convergence is ensured by a number of conditions simple to verify [GEM 84, HAS 70]. However, difficulties of implementation may appear due to the extended calculation time, to the need to establish a convergence diagnosis sometimes sophisticated of simulation algorithms [BRO 98], and to the additional work cost required to address issues of model selection based on the samples of the *a posteriori* distribution [MAR 07]. These considerations have prompted us to develop deterministic approximations, as a matter of fact variational, of the distribution [1.7]. Unlike MCMC schemas, variational calculation techniques are generally not accurate even asymptotically but their computational flexibility often justify their use.

The main idea here consists in approaching the target distribution, that is to say, the *a posteriori* distribution with a distribution for which the calculations

inherent to a maximization likelihood algorithm can be achieved, such as the EM algorithm (*Expectation Maximization*) [DEM 77]. The identification of the best distribution approximating the target distribution is performed relatively to the Kullback-Leibler divergence by imposing additional constraints when the target distribution is not directly computable. The most common procedure thus consists in assuming a product form for the approximating distribution as we will now illustrate in the JDE model.

In addition to the approximation based on a variational principle, the difference with the previous approach resides in the lack of *a priori* of the parameters. We are here considering a non-Bayesian framework with *missing variables*. The variables of interest considered as missing are A, h_γ, Q whereas L and Θ hold the status of parameters estimated by maximum likelihood in an iterative scheme such as *Expectation Maximization* (EM) [DEM 77]. It should be noted that from the perspective of the probabilistic process, there is no difference between a missing variable and a parameter with an *a priori* distribution such that it is easy to incorporate it to certain parameters if necessary. We will illustrate this flexibility in the following by adding an *a priori* to the spatial regularization parameters β_m.

1.5.2. *Variational EM algorithm*

We are looking for an approximation in the form $\widetilde{p} = \widetilde{p}_A \, \widetilde{p}_{H_\gamma} \, \widetilde{p}_Q$ of the target *a posteriori* distribution $f_{H_\gamma AQ} = p(h_\gamma, A, Q \,|\, Y; \Theta)$[9] minimizing the Kullback-Leibler divergence $\mathcal{D}(\widetilde{p} \| f_{H_\gamma AQ})$:

$$\mathcal{D}(\widetilde{p} \| f_{H_\gamma AQ}) = \int \widetilde{p}(h_\gamma, A, Q) \ln \frac{\widetilde{p}(h_\gamma, A, Q)}{f_{H_\gamma AQ}(h_\gamma, A, Q)} \, dh_\gamma \, dA \, dQ \qquad [1.11]$$

or equivalently by maximizing the free energy $\mathcal{F}(\widetilde{p}; \Theta) = \ln p(Y; \Theta) - \mathcal{D}(\widetilde{p} \| f_{H_\gamma AQ})$ [NEA 98]. The terms of the optimal distribution then verify:

$$(\widetilde{p}_A, \widetilde{p}_{H_\gamma}, \widetilde{p}_Q) = \arg\max_{p_H, p_A, p_Q} \mathcal{F}(p_A \, p_H \, p_Q; \Theta)$$

which is again simplified due of the product form but results in formulas that remain coupled and for which explicit direct solutions for $\widetilde{p}_A$, $\widetilde{p}_{H_\gamma}$ and $\widetilde{p}_Q$ are not available. However, the above formulation has the advantage of leading to an iterative solution in which one of the terms $\widetilde{p}_A$ is successively updated, $\widetilde{p}_{H_\gamma}$ and $\widetilde{p}_Q$ as follows, the two

---

9. The use of the semicolon makes it possible to distinguish unknown deterministic parameters in a parameters or random variable probabilistic model.

others being fixed:

stage E-H: $\quad \widehat{p}_{H_\gamma}^{(r)} = \underset{p_{H_\gamma}}{\arg\max}\, \mathcal{F}(\widehat{p}_A^{(r-1)}\, p_{H_\gamma}\, \widehat{p}_Q^{(r-1)}; \boldsymbol{\Theta}^{(r-1)})$ $\qquad$ [1.12]

stage E-A: $\quad \widehat{p}_A^{(r)} = \underset{p_A}{\arg\max}\, \mathcal{F}(p_A\, \widehat{p}_{H_\gamma}^{(r)}\, \widehat{p}_Q^{(r-1)}; \boldsymbol{\Theta}^{(r-1)})$ $\qquad$ [1.13]

stage E-Q: $\quad \widehat{p}_Q^{(r)} = \underset{p_Q}{\arg\max}\, \mathcal{F}(\widehat{p}_A^{(r)}\, \widehat{p}_{H_\gamma}^{(r)}\, p_Q; \boldsymbol{\Theta}^{(r-1)})$ $\qquad$ [1.14]

by noting $\widehat{p}_A^{(r-1)}$, $\widehat{p}_Q^{(r-1)}$ and $\boldsymbol{\Theta}^{(r-1)}$, common solutions and parameters at $r-1$. The expressions [1.12]-[1.14] can then be written in terms of the Kullback-Leibler divergence whose properties enables the identification of solution distributions as follows:

$$\widehat{p}_{H_\gamma}^{(r)}(\boldsymbol{h}_\gamma) \propto \exp\left(\mathrm{E}_{\widehat{p}_A^{(r-1)}\widehat{p}_Q^{(r-1)}}\left[\ln p(\boldsymbol{h}_\gamma\,|\,\boldsymbol{Y},\boldsymbol{A},\boldsymbol{Q};\boldsymbol{\Theta}^{(r-1)}]\right] \right) \qquad [1.15]$$

$$\widehat{p}_A^{(r)}(\boldsymbol{A}) \propto \exp\left(\mathrm{E}_{\widehat{p}_{H_\gamma}^{(r)}\widehat{p}_Q^{(r-1)}}\left[\ln p(\boldsymbol{A}\,|\,\boldsymbol{Y},\boldsymbol{h}_\gamma,\boldsymbol{Q};\boldsymbol{\Theta}^{(r-1)})\right] \right) \qquad [1.16]$$

$$\widehat{p}_Q^{(r)}(\boldsymbol{Q}) \propto \exp\left(\mathrm{E}_{\widehat{p}_A^{(r)}\widehat{p}_{H_\gamma}^{(r)}}\left[\ln p(\boldsymbol{Q}\,|\,\boldsymbol{Y},\boldsymbol{h}_\gamma,\boldsymbol{A};\boldsymbol{\Theta}^{(r-1)})\right] \right) \qquad [1.17]$$

With respect to the estimation of the parameters $\boldsymbol{\Theta}$, updates are performed according to:

$$\boldsymbol{\Theta}^{(r)} = \underset{\boldsymbol{\Theta}}{\arg\max}\, \mathrm{E}_{\widehat{p}_A^{(r)}\widehat{p}_{H_\gamma}^{(r)}\widehat{p}_Q^{(r)}}\left[\ln p(\boldsymbol{Y},\boldsymbol{h}_\gamma,\boldsymbol{A},\boldsymbol{Q}\,;\,\boldsymbol{\Theta})\right] \qquad [1.18]$$

Distribution expressions $\widehat{p}_{H_\gamma}^{(r)}$, $\widehat{p}_A^{(r)}$ and $\widehat{p}_Q^{(r)}$ prove to be explicit, as well as those of part of the parameters $\boldsymbol{\Theta}$. In particular, distributions $\widehat{p}_{H_\gamma}^{(r)}$ and $\widehat{p}_A^{(r)}$ are Gaussian. In the following text, to alleviate notations, we eliminate the exponent r and we note $\widetilde{p}_{H_\gamma} = \mathcal{N}(\boldsymbol{m}_{H_\gamma},\boldsymbol{V}_{H_\gamma})$ and $\widetilde{p}_A = \prod_j \widetilde{p}_{A_j}$ with $\widetilde{p}_{A_j} = \mathcal{N}(\boldsymbol{m}_{A_j},\boldsymbol{V}_{A_j})$. The expressions of $\boldsymbol{m}_{H_\gamma}$ et $\boldsymbol{V}_{H_\gamma}$ are similar to those obtained with the MCMC procedure in equation [1.8]. The terms which in [1.8] depend on a_j^m are replaced by their expectation with respect to the distribution $\widetilde{p}_A$. From [1.15], it is obtained:

$$\boldsymbol{m}_{H_\gamma} = \boldsymbol{V}_{H_\gamma} \sum_{j=1}^{J_\gamma} \widetilde{\boldsymbol{S}}_j^{\mathrm{t}}\boldsymbol{\Gamma}_j^{-1}(\boldsymbol{y}_j - \boldsymbol{P}\widetilde{\boldsymbol{\ell}}_j) \qquad [1.19]$$

$$\boldsymbol{V}_{H_\gamma}^{-1} = v_{\boldsymbol{h}}^{-1}\boldsymbol{R}^{-1} + \sum_{j=1}^{J_\gamma}\left(\sum_{m,m'} v_{A_j^m A_j^{m'}}\boldsymbol{X}_m^{\mathrm{t}}\boldsymbol{\Gamma}_j^{-1}\boldsymbol{X}_{m'} + \widetilde{\boldsymbol{S}}_j^{\mathrm{t}}\boldsymbol{\Gamma}_j^{-1}\widetilde{\boldsymbol{S}}_j \right) \qquad [1.20]$$

where $\widetilde{\boldsymbol{S}}_j = \sum_{m=1}^{M} m_{A_j^m} \boldsymbol{X}_m$. Notations $m_{A_j^m}$ and $v_{A_j^m A_j^{m'}}$ respectively represent components m and (m,m') of the mean vector and of the covariance matrix of the current distribution $\widetilde{p}_{A_j}$. In the case of the distribution $\widetilde{p}_{A_j}$ defined in $\mathbb{R}^M$, it yields:

$$\boldsymbol{m}_{A_j} = \boldsymbol{V}_{A_j} \left(\sum_{i=0,1} \boldsymbol{\Delta}_{ij}\boldsymbol{\mu}_i + \widetilde{\boldsymbol{G}}^{\mathrm{t}}\boldsymbol{\Gamma}_j^{-1}(\boldsymbol{y}_j - \boldsymbol{P}\boldsymbol{\ell}_j) \right) \qquad [1.21]$$

$$\boldsymbol{V}_{A_j} = \left(\sum_{i=0,1} \boldsymbol{\Delta}_{ij} + \widetilde{\boldsymbol{H}}_j \right)^{-1} \qquad [1.22]$$

where $\boldsymbol{\mu}_i = [\mu_{i,1}, \ldots, \mu_{i,M}]^{\mathrm{t}}$, $\widetilde{\boldsymbol{G}} = \mathrm{E}_{\widetilde{p}_{H_\gamma}}[\boldsymbol{G}]$ with $\boldsymbol{G} = [\boldsymbol{g}_1, \ldots, \boldsymbol{g}_M]$ (the column m of $\widetilde{\boldsymbol{G}}$ is denoted $\widetilde{\boldsymbol{g}}_m = \boldsymbol{X}_m \boldsymbol{m}_{H_\gamma}$), $\boldsymbol{\Delta}_{ij} = \mathrm{diag}[\widetilde{p}_{Q_j^m}(i)/\widetilde{v}_{i,m}]$ and $\widetilde{\boldsymbol{H}}_j = \mathrm{E}_{\widetilde{p}_{H_\gamma}}[\boldsymbol{G}^{\mathrm{t}}\boldsymbol{\Gamma}_j^{-1}\boldsymbol{G}]$, a matrix $M \times M$ whose element (m, m') is:

$$\mathrm{E}_{\widetilde{p}_{H_\gamma}}[\boldsymbol{g}_m^{\mathrm{t}}\boldsymbol{\Gamma}_j^{-1}\boldsymbol{g}_{m'}] = \mathrm{E}_{\widetilde{p}_{H_\gamma}}[\boldsymbol{g}_m]^{\mathrm{t}}\boldsymbol{\Gamma}_j^{-1}\mathrm{E}_{\widetilde{p}_{H_\gamma}}[\boldsymbol{g}_{m'}] + \mathrm{tr}\big(\boldsymbol{\Gamma}_j^{-1}\mathrm{cov}_{\widetilde{p}_{H_\gamma}}(\boldsymbol{g}_m, \boldsymbol{g}_{m'})\big)$$
$$= \widetilde{\boldsymbol{g}}_m^{\mathrm{t}}\boldsymbol{\Gamma}_j^{-1}\widetilde{\boldsymbol{g}}_{m'} + \mathrm{tr}\big(\boldsymbol{\Gamma}_j^{-1}\boldsymbol{X}_m \boldsymbol{V}_{H_\gamma} \boldsymbol{X}_{m'}^{\mathrm{t}}\big)$$

In this case, the similarity with updates obtained by MCMC is less obvious. In MCMC as a matter of fact, a_j^m are simulated in turns and conditionally to q_j^m and other $a_j^{m'}$. In the variational EM algorithm (VEM), marginals are calculated and integration is performed with regard to the other variables (q_j^m). However, a way to show consistency with the times [1.9] of the conditional Gaussian distribution $p(a_j^m \,|\, q_j^m = i, \boldsymbol{y}_j, \ldots)$ is to assume the equivalent of $q_j^m = i$, that is to say, $\widetilde{p}_{Q_j^m}(i) = 1$ and $\widetilde{p}_{Q_j^m}(1-i) = 0$. In equation [1.22] of the variance, the m-th diagonal term of $\sum_i \boldsymbol{\Delta}_{ij} + \widetilde{\boldsymbol{H}}_j$ is then equal to $v_{i,m}^{-1} + \widetilde{\boldsymbol{g}}_m^{\mathrm{t}}\boldsymbol{\Gamma}_j^{-1}\widetilde{\boldsymbol{g}}_m + \mathrm{tr}(\boldsymbol{\Gamma}_j^{-1}\boldsymbol{X}_m \boldsymbol{V}_{H_\gamma}\boldsymbol{X}_m^{\mathrm{t}})$. It can be observed in the first two terms that an expression similar to [1.9] reappears with a third additional term.

In the case of the average, the m-th diagonal term of $\sum_i \boldsymbol{\Delta}_{ij}\boldsymbol{\mu}_i + \widetilde{\boldsymbol{G}}^{\mathrm{t}}\boldsymbol{\Gamma}_j^{-1}(\boldsymbol{y}_j - \boldsymbol{P}\boldsymbol{\ell}_j)$ in [1.21] est $i\,\mu_{i,m}\, v_{i,m}^{-1} + \widetilde{\boldsymbol{g}}_m^{\mathrm{t}}\boldsymbol{\Gamma}_j^{-1}(\boldsymbol{y}_j - \boldsymbol{P}\boldsymbol{\ell}_j)$. Thus, the second factor appears once again in the expression [1.9] when replacing $\boldsymbol{g}_m$ par $\widetilde{\boldsymbol{g}}_m$ and up to the term $\sum_{m'\neq m} a_j^{m'}\boldsymbol{g}_{m'}$. It is in this last term that conditioning by $a_j^{m'}$, non-existing in the variational formulation, is expressed, as well as the interaction between the different conditions. It is carried out naturally by means of conditioning by $a_j^{m'}$ in MCMC whereas that it achieved by more complex matrix expressions and additional terms in VEM.

With respect to $\widetilde{p}_{\boldsymbol{Q}}$, the variables $(\boldsymbol{a}^m, \boldsymbol{q}^m)$ constitute independent pairs whose respective *a priori* distributions are hidden Ising models respectively with interaction parameter β_m, without external field and with Gaussian emission distributions. It follows that $\widetilde{p}_{\boldsymbol{Q}}(\boldsymbol{Q})$ has a product form: $\widetilde{p}_{\boldsymbol{Q}}(\boldsymbol{Q}) = \prod_m \widetilde{p}_{Q^m}(\boldsymbol{q}^m)$ with

$\widetilde{p}_{Q^m}(\boldsymbol{q}^m) = f(\boldsymbol{q}^m \,|\, \boldsymbol{a}^m = \boldsymbol{m}_{A^m}; \boldsymbol{\mu}_{.,m}, \boldsymbol{v}_{.,m}, \beta_m)$ where the right member represents the conditional distribution for a joint distribution noted f which is the distribution of a hidden Ising field modified relatively to the *a priori* hidden Ising field $(\boldsymbol{a}^m, \boldsymbol{q}^m)$. The modification consists in replacing the comments a_j^m by their mean $m_{A_j^m}$ (which become the new observations) and in adding an external field for $j \in J_\gamma$ and $i \in \{0,1\}$, $\alpha_{i,j} = -v_{A_j^m A_j^m}/v_{i,m}$, the remaining regularization parameter β_m. However the expression of the modified hidden Ising is not available explicitly due to the partition function. However, it is still possible to find a variational approximation, also known as mean-field, as specified in [CEL 03]. It is tantamount to consider the achieved approximation: $\widetilde{p}_{Q^m}(\boldsymbol{q}^m) \approx \prod_j \widetilde{p}_{Q^m}(q_j^m \,|\, \{\tilde{q}_k^m, k \sim j\})$ with $\tilde{\boldsymbol{q}}^m$ a field of fixed values that verifies a fixed point equation to solve. This solves the problem because the above conditional distributions for the hidden Ising field $\widetilde{p}_{Q^m}$ are now calculable. Furthermore, by applying the principle of the mean field, the $\tilde{q}_k^m$ is interpreted as the mean values of the hidden Ising fields at each site k. Other approximations are possible (see [CEL 03]).

Relatively to the update of the parameters $\boldsymbol{\Theta}$, the expression [1.18] gives rise to four independent updates. The first two are self-explanatory. It should be noted $\bar{p}_{im} = \sum_j \widetilde{p}_{Q_j^m}(i)$ for $i \in \{0,1\}$. It gives:

$$\mu_{i,m} = \sum_{j=1}^{J_\gamma} \frac{\widetilde{p}_{Q_j^m}(i)}{\bar{p}_{im}} m_{A_j^m}, \quad v_{i,m} = \sum_{j=1}^{J_\gamma} \frac{\widetilde{p}_{Q_j^m}(i)}{\bar{p}_{im}} \left((m_{A_j^m} - \mu_{i,m})^2 + v_{A_m^j A_m^j} \right)$$

$$v_{\boldsymbol{h}} = (D-1)^{-1} \mathrm{E}_{\widetilde{p}_{H_\gamma}}\left[\boldsymbol{h}_\gamma^{\mathrm{t}} R^{-1} \boldsymbol{h}_\gamma\right] = (D-1)^{-1}(\boldsymbol{m}_{H_\gamma}^{\mathrm{t}} R^{-1} \boldsymbol{m}_{H_\gamma} + \mathrm{tr}(\boldsymbol{V}_{H_\gamma} \boldsymbol{R}^{-1}))$$

$$= (D-1)^{-1}\mathrm{tr}((\boldsymbol{V}_{H_\gamma} + \boldsymbol{m}_{H_\gamma}\boldsymbol{m}_{H_\gamma}^{\mathrm{t}})\boldsymbol{R}^{-1})$$

With respect to Gaussian parameters and for a comparison with MCMC procedures, the *a posteriori* distributions obtained for these parameters can be referred to such as detailed in [VIN 10b, annexe A]. Recalling the notations in [VIN 10b], when in the above formulas $\widetilde{p}_{Q_j^m}(1) = 1$ is given for j such that $q_j^m = 1$ in the MCMC procedure, $\mu_{1,m} = \sum_{j \in C_{1,m}} m_{A_j^m}/J_{1,m}$ is met once more. This is consistent with the expression of $\eta_{1,m}$ (see [VIN 10b, equation (A.4)]) when replacing a_j^m by $m_{A_j^m}$ (in variational, the hyperparameter a_{μ_1} does not have to be included). Respectively to variances, it gives $v_{i,m} = \sum_{j \in C_{i,m}} ((m_{A_j^m} - \mu_{i,m})^2 + v_{A_j^m A_j^m})/J_{i,m}$, which up to the term $v_{A_j^m A_j^m}$ is consistent with the mean (see [VIN 10b, equation (A.4)]) of the inverse-gamma distribution $v_{i,m}$ in the MCMC procedure. Also the fact that in MCMC, conditioning is achieved for these calculations by a_j^m, the observed differences are due to the presence of hyperparameters and to *a priori* distributions that do not exist in the VEM algorithm discussed here.

For $v_{\boldsymbol{h}}$ there is in VEM an expression consistent with the simulation of $v_{\boldsymbol{h}}$ in MCMC (see [MAK 08, paragraph B.1]). While $v_{\boldsymbol{h}}$ is conditionally simulated with

$\boldsymbol{h}_\gamma$ fixed to its current value in MCMC, the expressions in $\boldsymbol{h}_\gamma$ are replaced by their expected values relatively to the current approximating distribution in VEM.

The other two updates (interaction parameters $\boldsymbol{\beta}$ and noise parameters) require an iterative maximization procedure. With respect to parameters β_m, the approximation created above [CEL 03] leads to an equation for which a gradient-based algorithm can be used. A tendency towards the overestimation of these parameters can then be observed . This can be partly compensated by introducing an *a priori* distribution $p(\beta_m)$ aiming to reduce the estimated value β_m. We thus illustrate the possibility mentioned previously to incorporate, as with the MCMC case, *a priori* distributions of the parameters. More specifically, if it is assumed that $p(\beta_m)$ is an exponential distribution with a parameter λ_m, it gives:

$$\beta_m = \arg\max_{\beta'_m} E_{\widetilde{p}_{Q^m}}[\ln p(\boldsymbol{q}^m \,|\, \beta'_m)p(\beta'_m)]$$

$$= \arg\max_{\beta'_m}\{-\ln Z(\beta'_m) + \beta'_m(\sum_{j\sim k} \mathrm{E}_{\widetilde{p}_{Q^m}}\left[I(q_j^m = q_k^m)\right] - \lambda_m)\}$$

If derivation is carried out with respect to β_m, the outcome is again then, the conventional expression detailed in [CEL 03] in which the constant λ_m is subtracted from the usual quantity $\sum_{j\sim k} \mathrm{E}_{\widetilde{p}_{Q^m}}\left[I(q_j^m = q_k^m)\right]$ representing the mean number of homogeneous cliques of the approximating distribution. It is easy to see that this subtraction has the effect of decreasing the value of β_m estimated as desired.

With regard to the parameters $\{\boldsymbol{\ell}_j, \sigma_j^2, \boldsymbol{\Lambda}_j, j = 1..J_\gamma\}$, they satisfy a fixed-point equation of that we do not fully detail. In the AR(1) case, it can be shown that:

$$\boldsymbol{\ell}_j = (\boldsymbol{P}^{\mathrm{t}}\boldsymbol{\Gamma}_j^{-1}\boldsymbol{P})^{-1}\boldsymbol{P}^{\mathrm{t}}\boldsymbol{\Gamma}_j^{-1}\big(\boldsymbol{y}_j - \widetilde{\boldsymbol{S}}_j\boldsymbol{m}_{H_\gamma}\big) = F_1(\rho_j) \tag{1.23}$$

Hence a similarity with [MAK 08, equation (B.2)] can be observed in [1.23] when replacing $\boldsymbol{h}_\gamma$ et $\boldsymbol{A}$ par $\boldsymbol{m}_{H_\gamma}$ and $\boldsymbol{m}_A$. In a similar manner, it can be shown that the optimal values verify two other relationships $\sigma_j^2 = F_2(\rho_j, \boldsymbol{\ell}_j)$ and $\rho_j = F_3(\rho_j, \sigma_j^2)$. This then allows these different relationships to combine to estimate ρ_j as a solution to a fixed point equation and to derive then $\boldsymbol{\ell}_j$ and σ_j.

1.6. Comparaison of both types of solutions

In order to compare the two methods, a number of simulations as well as experiments on real data have been carried out [CHA 11a].

Experiments on simulated data. Firstly, we have simulated data from the equation [1.1] and the $p(\boldsymbol{A} \,|\, \boldsymbol{Q})$ distribution with a matrix $\boldsymbol{P}$ defined as a discrete cosine transform basis, white Gaussian noise ($\sigma_j^2 = 0{,}5$, $\boldsymbol{\Lambda}_j = \boldsymbol{I}_N$) and

$M = 2$ experimental conditions with variable contrast-to-noise ratios (CNR). More specifically, we have set: $\mu_{1,1} = 2{,}8$, $v_{1,1} = 0{,}3$ and $\mu_{1,2} = 1{,}8$, $v_{1,2} = 0{,}4$, such that $\mu_{1,1}/v_{1,1} > \mu_{1,2}/v_{1,2}$. The other variances $v_{0,\cdot}$ are set to 0.3. Using this mixture, the artificial NRLs are generated conditionally to synthetic binary images of size 20×20 representing activated and non-activated pixels (figure 1.6). In addition, the initial paradigm is constituted of fifteen stimuli for each of the conditions. Simulated data are thus constituted of 152 scans time series.
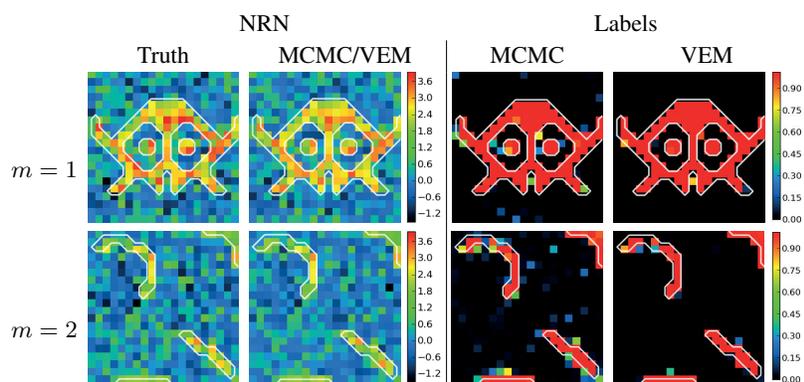
Figure 1.6. *On the left: NRLs simulated and estimated by MCMC and VEM (very similar results);*
on the right: a posteriori probability maps obtained by the approximation $\widetilde{p}_{\boldsymbol{Q}_m}$ (VEM) and by the MMAP estimator $\widehat{\boldsymbol{q}}^m$ (MCMC) (see color annex)

The two MCMC and VEM procedures are then applied to these data. We are under the scope of the true noise model, that is to say, white Gaussian as in simulations. Both approaches produce very similar NRLs. A slight difference is observed in the *a posteriori* activation probabilities of the condition with a low CNR ($m = 2$). These probabilities are given by $p_{Q_j^m}(1)$ in the variational case and by $\hat{q}_j^m(1)$ defined in Section 1.4 in the MCMC case. This difference suggests a gain in robustness in favor of the variational approach. The estimated levels of spatial regularization also differ with $\widehat{\beta}_1 = 0{,}78$, $\widehat{\beta}_2 = 0{,}92$ for MCMC and $\widehat{\beta}_1 = 1{,}04$, $\widehat{\beta}_2 = 1{,}08$ for VEM.

For a more quantitative comparison, additional simulations have been performed with varying stimuli densities (from five to thirty), variable noise variances and different temporal correlation models for the noise (AR structure for $\boldsymbol{\Lambda}_i$). The results are shown in Fig. 1.7 that shows (a) the evolution of the mean squared error (MSE) of NRLs estimated based on the number of stimuli for simulations following a AR(2) noise model such that the estimation assumes a white Gaussian noise as previously.

Fig. 1.7 shows that for a low stimuli density, that is to say, for a low signal-to-noise ratio (SNR), the variational version is more robust. In the case of higher
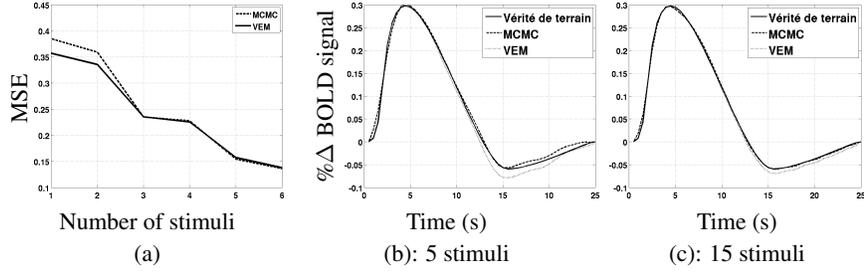
Figure 1.7. *(a) Evolution of the MSE of the NRLs as a function of the number of stimuli,*
(b)-(c) ground truth and HRF estimated with VEM inferences and MCMC
*for two different stimuli densities, using an A(2) noise*

densities (higher than twenty) the two approaches behave in the same manner. On the other hand, Fig. 1.7b and 1.7c show for two densities from different stimulations (five and fifteen) the HRFs estimated with respect to the canonical HRF used for simulation. The main features (peak value, arrival times at the peak and *undershoot*) are correctly estimated by the two approaches. However, we observe in Fig. 1.7b shows that for a low stimuli density, the variational approach is less accurate than its stochastic counterpart at the *undershoot* level. This observation is also confirmed when the three above characteristics of the real HRF used in the simulations are varied. However, when estimations and simulations are made with the same noise model, the differences observed between the two approaches are minimal and not significant.

Figures 1.8a and 1.8b show the evolution of the MSE of NRLs depending on the NSR when the variance of the noise and autocorrelation are respectively varied.

In the latter case, the two parameters of the AR(2) model are modified in such a way as to maintain a stable AR process. Similarly as already observed in [CAS 08], for a given NSR, a larger autocorrelation implies an increase of the MSE more significant than the increase of the noise variance, and this for both approaches. Moreover, the two methods behave in the same manner over a large range of values for RSB $\geqslant$ 5,5 dB.

Finally, the most notable advantage of the variational approach reside in calculations times. On a Core 2 - 2,26 GHz - 2 Gb RAM Intel architecture, results have been obtained approximately thirty times faster.

Experiments on real data. We have also considered real fMRI data output from a 3T MRI (Siemens Trio) with a gradient echo sequence EPI (TE $=$ 30 ms/TR $=$ 2,4 s/FOV $=$ 192 mm^2) and a paradigm resulting from a *Localizer* protocol [PIN 07]. The acquisition carried out includes a single session of $N = 128$ 3D volumes scans with a $2 \times 2 \times 3$ mm^3 resolution. The paradigm includes ten conditions (heard and
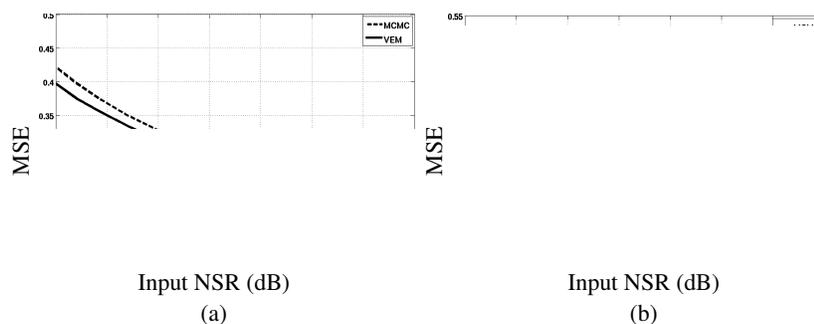
Figure 1.8. *Evolution of the MSE of the NRLs as a function of the input NSR (AR(2) noise) (a) by varying noise variance and (b) the correlation level of AR(2) noise*

read sentences, aurally induced and read calculations, left and right clicks aurally and visually induced, horizontal and vertical checkerboards) divided into sixty stimuli.

We have focused on the contrast `calculation-sentence` (combined auditory and visual stimuli) taking into account the differences of activations induced by the calculation and the sentence conditions in the left intraparietal sulcus, subdivided into 17 parcels for JDE analyses. The choice of this region lies in the fact that it is likely to induce a HRF which deviates from the canonical form. An extended version of these results is presented in [CHA 13].

Figure 1.9 shows that NRLs estimated by both approaches are very similar and follow in a satisfactory manner the underlying anatomy of the furrows. It should be noted here that only the most activated cut is visualized in Fig. 1.9, where we also show the two estimations (MCMC and VEM) of the HRF in the most activated parcel that includes approximately 200 voxels. The HRF are similar in both approaches and clearly deviate from the canonical form particularly at the level of the time of arrival at the peak and at the *undershoot*, that is, postactivation depletion. The variational approach generates a HRF which oscillates more at the level of this depletion but this is tempered by the fact that in a general fashion, the estimation the tail of the HRF is less reliable than the peak for which the BOLD signal level is more important. In addition, the event-based nature of the paradigm under consideration here is not adapted to precisely study the characteristics of the tail of the HRF. With a slow event paradigm for which responses do not overlap in time, our tests show that these oscillations disappear. A pragmatic solution proposed to solve this issue in the framework of fast event-related paradigms consists of introducing in the design of the paradigm zero events, that is to say slightly longer periods without stimulation, such as to allow time for the hemodynamics response to recover its base line. Another way consists in restraining the HRF model using a semi-parametric approach as in [GEN 00, WOO 04a].

$$\widehat{\beta}_{\text{calcul}} \qquad \widehat{\beta}_{\text{phrase}} \qquad \widehat{\beta}_{\text{calcul}} \qquad \widehat{\beta}_{\text{phrase}}$$
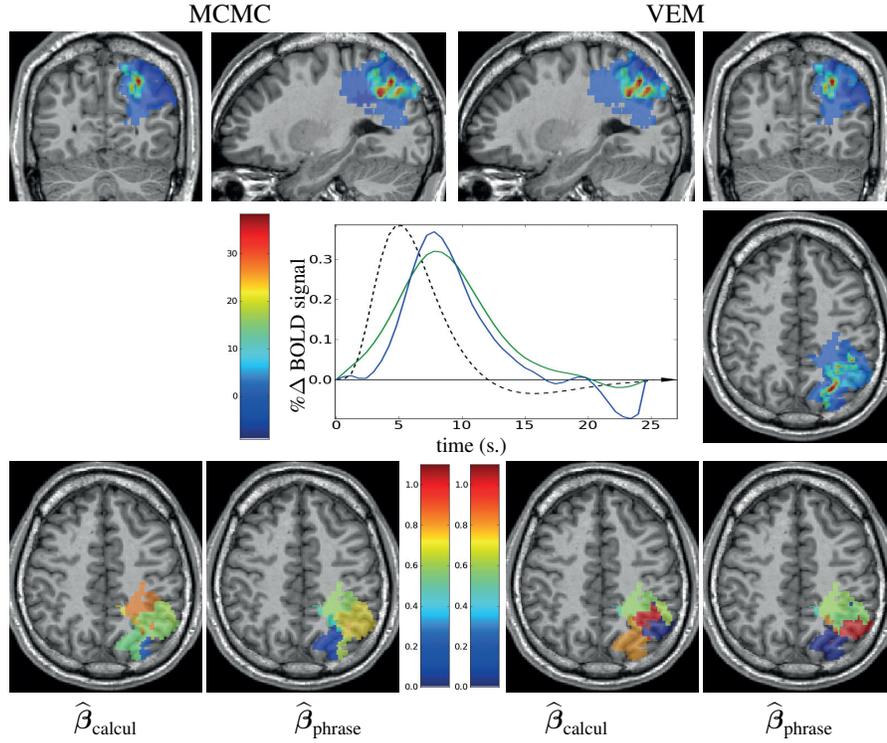
Figure 1.9. *Coronal (top row, exterior), sagittal (top row, center) and axial (middle row) views of the* `calculation-sentence` *contrast estimated by MCMC JDE (on the left) and VEM (on the right). At the center: HRF estimated by MCMC (in green) and by VEM (in blue) and HRF canonical in dashed. Bottom row maps of spatial regularization levels estimated for the conditions* `calculation` *and* `sentence` *by MCMC (left) and by VEM (right) (see color annex).*

On the other hand, the estimated spatial regularization levels, as shown in the maps at the bottom of Fig. 1.9, are significantly different from an approach to the other, with stronger estimated levels for VEM. However, for the most activating parcel, it can be noted that for both approaches there is coherence with the contrast achieved: the value of $\widehat{\beta}$ is stronger for the `calculation` condition than for the `sentence` condition. Finally, respectively to calculation times, in the study of this parcel, a same gain by a factor of 30 for the variational approach as for simulations can be observed.

1.7. Conclusion

The experiments described in the previous section aimed essentially to compare both VEM and MCMC approaches proposed for the estimation of the JDE model.

More detailed results with the JDE approach itself and its comparison with other models can also be found in [BAD 11].

The results of Section 1.6 confirm the conventional advantages of the variational approach, namely the simplicity of implementation, the speed of calculations, etc. With respect to the comparison with the MCMC procedure, what appears as particularly advantageous is the simplicity of the convergence criterion in variational and the possibility to relatively easily extend the procedure to more complex models including for example AR noises of higher order or a model of neural habituation. Aspects of model selection are also accessible if considering penalized likelihood-based criteria whose variational approach can easily provide an approximation [FOR 03].

With regard to performance, they are often very similar for the two inference schemes, if the interest is as here towards point estimators. However, significant differences appear in the uncertainty measures of these estimators, that is to say, in the estimation variances.

This result with point estimators may seem surprising to the extent where only the MCMC procedure offers guarantees of theoretical convergence but in reality it can hide different situations. On the one hand, this does not exclude that the variational approach has also in some cases the same convergence properties but so far there exist no fairly general results about the quality of these approximations. On the other hand, it is not excluded that simplifications introduced in the variational approach of the factorization of the target distribution induce a greater robustness regarding certain model errors (response stationarity, noise, etc.).

In the specific case of the JDE, a more in-depth study by means of simulations could be envisaged in order to try to better identify at which stage of the model the variational approximation is the most active and potentially indicate if this action is prone to important errors or not. Another interesting aspect observed in our simulations, and which is not contradictory to the approximation aspect, is the greater robustness of the variational approach to model errors.

Finally, to complete the comparison of approaches and the evaluation of the potential of the variational solution, it would be interesting to carry out a group analysis with it such as the one achieved with the MCMC procedure in [BAD 11].

1.8. Bibliographie

[AGU 98] AGUIRRE G., ZARAHN E., D'ESPOSITO M., "The variability of human, BOLD hemodynamic responses", *Neuroimage*, vol. 8, p. 360-369, 1998.

[BAD 11] BADILLO S., VINCENT T., CIUCIU P., "Impact of the joint detection-estimation approach on random effects group studies in fMRI", *IEEE International Symposium on Biomedical Imaging*, Chicago, IL, Etats-Unis, p. 376-380, avr. 2011.

[BAI 97] BAILLET S., GARNERO L., "A Bayesian approach to introducing anatomo-functional priors in the EEG/MEG inverse problem", *IEEE Transactions on Biomedical Engineering*, vol. 44, n° 5, p. 374-385, mai 1997.

[BAK 12] BAKHOUS C., FORBES F., VINCENT T., CHAARI L., DOJAT M., CIUCIU P., "Adaptive experimental condition selection in event-related fMRI", *IEEE International Symposium on Biomedical Imaging*, Barcelona, Spain, p. 1755-1758, mai 2012.

[BAU 11] BAUSCHKE H. H., COMBETTES P. L., *Convex Analysis and Monotone Operator Theory in Hilbert Spaces*, CMS books in Mathematics, Springer, 2011.

[BOY 12] BOYER C., CIUCIU P., WEISS P., MÉRIAUX S., "HYR^{2}PICS: Hybrid regularized reconstruction for combined parallel imaging and compressive sensing in MRI", *IEEE International Symposium on Biomedical Imaging*, Barcelona, Spain, p. 66-69, mai 2012.

[BRO 98] BROOKS S. P., GELMAN A., "General Methods for Monitoring Convergence of Iterative Simulations", *Journal of Computational and Graphical Statistics*, vol. 7, n° 4, p. 434-455, 1998.

[BUC 98] BUCKNER R., "Event-related fMRI and the hemodynamic response", *Human Brain Mapping*, vol. 6, n° 5-6, p. 373-377, 1998.

[BUX 98] BUXTON R. B., WONG E. C., FRANK L. R., "Dynamics of blood flow and oxygenation changes during brain activation: the balloon model", *Magnetic Resonance in Medecine*, vol. 39, p. 855-864, juin 1998.

[BUX 04] BUXTON R. B., ULUDAĞ K., DUBOWITZ D. J., LIU T. T., "Modeling the hemodynamic response to brain activation", *Neuroimage*, vol. 23, Supplement 1, p. S220-S233, 2004.

[CAS 08] CASANOVA R., RYALI S., SERENCES J., YANG L., KRAFT R., LAURIENTI P. J., MALDJIAN J. A., "The impact of temporal regularization on estimates of the BOLD hemodynamic response function: a comparative analysis", *Neuroimage*, vol. 40, n° 4, p. 1606-1618, mai 2008.

[CEL 03] CELEUX G., FORBES F., PEYRARD N., "EM procedures using mean field-like approximations for Markov model-based image segmentation", *Pattern Recognition*, vol. 36, p. 131-144, 2003.

[CHA 11a] CHAARI L., FORBES F., VINCENT T., DOJAT M., CIUCIU P., "Variational solution to the joint detection estimation of brain activity in fMRI", *MICCAI*, LNCS 6892, Toronto, Canada, Springer, Berlin, p. 260-268, sep. 2011.

[CHA 11b] CHAARI L., PESQUET J.-C., BENAZZA-BENYAHIA A., CIUCIU P., "A wavelet-based regularized reconstruction algorithm for SENSE parallel MRI with applications to neuroimaging", *Medical Image Analysis*, vol. 15, n° 2, p. 185-201, 2011.

[CHA 13] CHAARI L., VINCENT T., FORBES F., DOJAT M., CIUCIU P., "Fast joint detection-estimation of evoked brain activity in event-related fMRI using a variational approach", *IEEE Transactions on Medical Imaging*, vol. 32, n° 5, p. 821-837, 2013.

[CIU 03] CIUCIU P., POLINE J.-B., MARRELEC G., IDIER J., PALLIER C., BENALI H., "Unsupervised robust non-parametric estimation of the hemodynamic response function for any fMRI experiment", *IEEE Transactions on Medical Imaging*, vol. 22, n° 10, p. 1235-1251, oct. 2003.

[CIU 04] CIUCIU P., IDIER J., ROCHE A., PALLIER C., "Outlier detection for robust region-based estimation of the hemodynamic response function in event-related fMRI", *IEEE International Symposium on Biomedical Imaging*, Arlington, VA, Etats-Unis, p. 392-395, avr. 2004.

[CIU 08] CIUCIU P., ABRY P., RABRAIT C., WENDT H., "Log wavelet leaders cumulant based multifractal analysis of EVI fMRI time series: evidence of scaling in ongoing and evoked brain activity", *IEEE Journal of Selected Topics in Signal Processing*, vol. 2, n° 6, p. 929-943, déc. 2008.

[CIU 12] CIUCIU P., VAROQUAUX G., ABRY P., SADAGHIANI S., KLEINSCHMIDT A., "Scale-free and multifractal time dynamics of fMRI signals during rest and task", *Frontiers in Physiology*, vol. 3, n° Article 186, p. 1-18, juin 2012.

[DAL 97] DALE A. M., BUCKNER R. L., "Selective averaging of rapidly presented individual trials using fMRI", *Human Brain Mapping*, vol. 5, p. 329-340, 1997.

[de 08] DE PASQUALE F., DEL GRATTA C., ROMANI G., "Empirical Markov Chain Monte Carlo Bayesian analysis of fMRI data", *Neuroimage*, vol. 42, n° 1, p. 99-111, août 2008.

[D'E 99] D'ESPOSITO M., ZARAHN E., AGUIRRE G. K., RYPMA B., "The effect of normal aging on the coupling of neural activity to the BOLD hemodynamic response", *Neuroimage*, vol. 10, n° 1, p. 6-14, juil. 1999.

[DEM 77] DEMPSTER A. P., LAIRD N. M., RUBIN D. B., "Maximum likelihood from incomplete data via the EM algorithm", *Journal of the Royal Statistical Society B*, vol. 39, p. 1-38, 1977.

[EKS 10] EKSTROM A., "How and when the fMRI BOLD signal relates to underlying neural activity: The danger in dissociation", *Brain Research Reviews*, vol. 62, n° 2, p. 233-244, 2010.

[FOR 03] FORBES F., PEYRARD N., "Hidden Markov random field selection criteria based on mean field-like approximations", *IEEE Transactions on Pattern Analysis and Machine Intelligence*, vol. 25, n° 8, p. 1089-1101, 2003.

[FOX 07] FOX M. D., RAICHLE M. E., "Spontaneous fluctuations in brain activity observed with functional magnetic resonance imaging", *Nature Reviews Neuroscience*, vol. 8, n° 9, p. 700-11, sep. 2007.

[FRI 95] FRISTON K., HOLMES A. P., POLINE J.-B., GRASBY P., WILLIAMS S., FRACKOWIAK R., TURNER R., "Analysis of fMRI time-series revisited", *Neuroimage*, vol. 2, p. 45-53, 1995.

[GEM 84] GEMAN S., GEMAN D., "Stochastic relaxation, Gibbs distributions, and the Bayesian restoration of images", *IEEE Transactions on Pattern Analysis and Machine Intelligence*, vol. PAMI-6, n° 6, p. 721-741, nov. 1984.

[GEN 00] GENOVESE C., "A Bayesian time-course model for functional magnetic resonance imaging data (with discussion)", *Journal of American Statistical Association*, vol. 95, p. 691-719, 2000.

[GOU 00] GOUTTE C., NIELSEN F. A., HANSEN L. K., "Modeling the haemodynamic response in fMRI using smooth filters", *IEEE Transactions on Medical Imaging*, vol. 19, n° 12, p. 1188-1201, déc. 2000.

[GRA 11] GRAMFORT A., STROHMEIER D., HAUEISEN J., HAMALAINEN M., KOWALSKI M., "Functional brain imaging with M/EEG using structured sparsity in time-frequency dictionaries", SZÉKELY G., HAHN H. K. (DIR.), *IPMI*, vol. 6801, Springer, Berlin, p. 600-611, 2011.

[GRE 03] GREICIUS M. D., KRASNOW B., REISS A. L., MENON V., "Functional connectivity in the resting brain: a network analysis of the default mode hypothesis", *Proceedings of the National Academy of Sciences of the United States of America*, vol. 100, n° 1, p. 253-258, jan. 2003.

[HAL 98] HALGREN E., MARINKOVIK K., CHAUVEL P., "Generators of the late cognitive potentials in auditory and visual oddball tasks", *Electroencephalography and Clinical Neurophysiology*, vol. 102, n° 2, p. 156-164, 1998.

[HAN 04] HANDWERKER D. A., OLLINGER J. M., D'ESPOSITO M., "Variation of BOLD hemodynamic responses across subjects and brain regions and their effects on statistical analyses", *Neuroimage*, vol. 21, p. 1639-1651, 2004.

[HAS 70] HASTINGS W. K., "Monte Carlo sampling methods using Markov chains and their applications", *Biometrika*, vol. 57, n° 1, p. 97-109, jan. 1970.

[HEN 00] HENSON R., ANDERSSON J., FRISTON K., "Multivariate SPM application to basis function characterisations of event-related fMRI responses", *Neuroimage*, vol. 11, p. 468, 2000.

[HIG 98] HIGDON D. M., "Auxiliary variable methods for Markov chain Monte Carlo with applications", *Journal of American Statistical Association*, vol. 93, n° 442, p. 585-595, juin 1998.

[KAY 88] KAY S. M., *Modern Spectral Estimation*, Prentice-Hall, Englewood Cliffs, NJ, Etats-Unis, 1988.

[LIN 01] LINKENKAER-HANSEN K., NIKOULINE V. V., PALVA J. M., ILMONIEMI R. J., "Long-range temporal correlations and scaling behavior in human brain oscillations", *The Journal of Neuroscience*, vol. 21, n° 4, p. 1370-1377, fév. 2001.

[LOG 01] LOGOTHETIS N. K., PAULS J., AUGATH M., TRINATH T., OELTERMANN A., "Neurophysiological investigation of the basis of the fMRI signal", *Nature*, vol. 412, n° 6843, p. 150-157, juil., 12 2001.

[LUS 07] LUSTIG M., DONOHO D., PAULY J., "Sparse MRI: The application of compressed sensing for rapid MR imaging", *Magnetic Resonance in Medecine*, vol. 58, n° 6, p. 1182-1195, déc. 2007.

[MAK 05] MAKNI S., CIUCIU P., IDIER J., POLINE J.-B., "Joint detection-estimation of brain activity in functional MRI: a multichannel deconvolution solution", *IEEE Transactions on Signal Processing*, vol. 53, n° 9, p. 3488-3502, sep. 2005.

[MAK 08] MAKNI S., IDIER J., VINCENT T., THIRION B., DEHAENE-LAMBERTZ G., CIUCIU P., "A fully Bayesian approach to the parcel-based detection-estimation of brain activity in fMRI", *Neuroimage*, vol. 41, n° 3, p. 941-969, juil. 2008.

[MAR 03] MARRELEC G., BENALI H., CIUCIU P., PÉLÉGRINI-ISSAC M., POLINE J.-B., "Robust Bayesian estimation of the hemodynamic response function in event-related BOLD MRI using basic physiological information", *Human Brain Mapping*, vol. 19, n° 1, p. 1-17, mai 2003.

[MAR 07] MARIN J.-M., ROBERT C. P., *Bayesian Core: A Practical Approach to Computational Bayesian Statistics*, Springer, fév. 2007.

[MIE 00] MIEZIN F. M., MACCOTTA L., OLLINGER J. M., PETERSEN S. E., BUCKNER R. L., "Characterizing the hemodynamic response: effects of presentation rate, sampling procedure, and the possibility of ordering brain activity based on relative timing", *Neuroimage*, vol. 11, p. 735-759, 2000.

[NEA 98] NEAL R., HINTON G., "A view of the EM algorithm that justifies incremental, sparse and other variants", JORDAN M. (DIR.), *Learning in Graphical Models*, p. 355-368, MIT Press, Cambridge, MA, Etats-Unis, 1998.

[OGA 90] OGAWA S., LEE T., KAY A., TANK D., "Brain magnetic resonance imaging with contrast dependent on blood oxygenation", *Proceedings of the National Academy of Sciences of the United States of America*, vol. 87, n° 24, p. 9868-9872, 1990.

[PEN 07] PENNY W., FLANDIN G., TRUJILLO-BARETO N., "Bayesian comparison of spatially regularised general linear models", *Human Brain Mapping*, vol. 28, n° 4, p. 275-293, 2007.

[PIN 07] PINEL P., THIRION B., MÉRIAUX S., JOBERT A., SERRES J., LE BIHAN D., POLINE J.-B., DEHAENE S., "Fast reproducible identification and large-scale databasing of individual functional cognitive networks", *BMC Neuroscience*, vol. 8, n° 1, p. 91, 2007.

[PRU 99] PRUESSMANN K. P., WEIGER M., SCHEIDEGGER M., BOESIGER P., "SENSE: Sensitivity encoding for fast MRI", *Magnetic Resonance in Medecine*, vol. 42, p. 952-962, Nov 1999.

[RIC 03] RICHTER W., RICHTER M., "The shape of the fMRI BOLD response in children and adults changes systematically with age", *Neuroimage*, vol. 20, n° 2, p. 1122-1131, 2003.

[RIE 04] RIERA J. J., WATANABE J., KAZUKI I., NAOKI M., AUBERT E., OZAKI T., KAWASHIMAA R., "A state-space model of the hemodynamic approach: nonlinear filtering of BOLD signals", *Neuroimage*, vol. 21, p. 547-567, 2004.

[RIS 11] RISSER L., VINCENT T., FORBES F., IDIER J., CIUCIU P., "Min-max extrapolation scheme for fast estimation of 3D Potts field partition functions. Application to the joint detection-estimation of brain activity in fMRI", *Journal of Signal Processing Systems*, vol. 65, n° 3, p. 325-338, déc. 2011.

[ROB 07] ROBERT C. P., *The Bayesian Choice: From Decision-Theoretic Foundations to Computational Implementation*, Springer, juin 2007.

[SEK 05] SEKIHARA K., SAHANI M., NAGARAJAN S. S., "Localization bias and spatial resolution of adaptive and non-adaptive spatial filters for MEG source reconstruction", *Neuroimage*, vol. 25, n° 4, p. 1056-1067, 2005.

[SMI 03] SMITH M., PÜTZ B., AUER D., FAHRMEIR L., "Assessing brain activity through spatial Bayesian variable selection", *Neuroimage*, vol. 20, p. 802-815, 2003.

[SWA 98] SWARTZ B., GOLDENSOHN E., "Timeline of the history of EEG and associated fields", *Electroencephalography and clinical Neurophysiology*, vol. 102, n° 2, p. 173-176, 1998.

[VIN 10a] VINCENT T., RISSER L., CIUCIU P., "Spatially adaptive mixture modeling for analysis of within-subject fMRI time series", *IEEE Transactions on Medical Imaging*, vol. 29, n° 4, p. 1059-1074, avr. 2010.

[VIN 10b] VINCENT T., Modèles hémodynamiques spatiaux adaptatifs pour l'imagerie cérébrale fonctionnelle, thèse de doctorat, université Paris-sud, Orsay, sep. 2010.

[WOO 01] WOOLRICH M., RIPLEY B., BRADY M., SMITH S., "Temporal autocorrelation in univariate linear modelling of fMRI data", *Neuroimage*, vol. 14, n° 6, p. 1370-1386, déc. 2001.

[WOO 04a] WOOLRICH M., JENKINSON M., BRADY J., SMITH S., "Fully Bayesian spatio-temporal modelling of fMRI data", *IEEE Transactions on Medical Imaging*, vol. 23, n° 2, p. 213-231, fév. 2004.

[WOO 04b] WOOLRICH M., JENKINSON M., BRADY J. M., SMITH S., "Constrained linear basis set for HRF modelling using variational Bayes", *Neuroimage*, vol. 21, n° 4, p. 1748-1761, 2004.

[ZAR 97] ZARAHN E., AGUIRRE G. K., D'ESPOSITO M., "Empirical analysis of BOLD fMRI statistics. I. Spatially unsmoothed data collected under null-hypothesis conditions", *Neuroimage*, vol. 5, n° 3, p. 179-197, avr. 1997.